Mon. Not. R. Astron. Soc. **000**, 000–000 (0000) Printed 16 July 2003 (MN LaTeX style file v2.2)

A fundamental plane of black hole activity

Andrea Merloni, Sebastian Heinz & Tiziana Di Matteo
Max-Planck-Institut für Astrophysik, Karl-Schwarzschild-Strasse 1, D-85741, Garching, Germany

ABSTRACT

We examine the disc–jet connection in stellar mass and supermassive black holes by investigating the properties of their compact emission in the X-ray and radio bands. We compile a sample of $\sim$100 active galactic nuclei with measured mass, 5 GHz core emission, and 2-10 keV luminosity, together with 8 galactic black holes with a total of $\sim$ 50 simultaneous observations in the radio and X-ray bands. Using this sample, we study the correlations between the radio ($L_{\rm R}$) and the X-ray ($L_{\rm X}$) luminosity and the black hole mass (M). We find that the radio luminosity is correlated with *both* M and $L_{\rm X}$, at a highly significant level. In particular, we show that the sources define a "fundamental plane" in the three-dimensional $(\log L_{\rm R}, \log L_{\rm X}, \log M)$ space, given by $\log L_{\rm R} = (0.60^{+0.11}_{-0.11}) \log L_{\rm X} + (0.78^{+0.11}_{-0.09}) \log M + 7.33^{+4.05}_{-4.07}$, with a substantial scatter of $\sigma_{\rm R} = 0.88$. We compare our results to the theoretical relations between radio flux, black hole mass, and accretion rate derived by Heinz & Sunyaev (2003). Such relations depend only on the assumed accretion model and on the observed radio spectral index. Therefore, we are able to show that the X-ray emission from black holes accreting at less than a few per cent of the Eddington rate is unlikely to be produced by radiatively efficient accretion, and is marginally consistent with optically thin synchrotron emission from the jet. On the other hand, models for radiatively inefficient accretion flows seem to agree well with the data.

Key words: accretion, accretion disks – black hole physics – X-rays: binaries – galaxies: active – radio continuum: general – X-rays: general

1 INTRODUCTION

The ultimate observational evidence of a celestial body being a black hole comes from dynamical studies, by measuring the gravitational influence of the central object on neighboring stars and gas, both in binary systems and in the nuclei of galaxies. However, there are a number of distinctive signatures of black hole-powered activity that are usually regarded as proxy of black hole existence. Relativistic jets emitting synchrotron radiation in the radio band are one such signature, the second most common being the presence of strong, compact power-law X-ray emission commonly associated with the inner part of an accretion flow[1]. Indeed, as a general property, accretion onto compact objects and the launch of relativistic outflows/jets seem to be correlated (or *symbiotic*, Falcke & Biermann, 1995) phenomena (Begelman, Blandford, & Rees 1984; Rawlings & Saunders 1991). This implies that, at some level, a correlation between jet and disc flux is unavoidable.

Observationally, jet morphologies and spectral properties of both radio and X-ray cores are remarkably similar in the case of black holes of stellar mass (galactic black holes, hereafter GBH) and of their supermassive counterparts in the nuclei of galaxies (hereafter SMBH). If jets are launched in the innermost parts of the accretion flows, as commonly assumed, then these similarities suggest that it should be possible to understand the physics of both black hole accretion and jet production by studying all those systems as a *single* class. To this end, radiation emerging at radio and (hard) X-ray frequencies is the most direct probe of the immediate vicinity of the black hole: effects of extinction are unimportant in the radio band, while in the X-rays, where a large fraction of the accretion energy is radiated, such effects can be accounted for with good enough spectral capabilities. Thus, radio and X-ray observations, together with the information on the central black hole mass, should allow us to study the relationship between the fundamental parameters characterizing black hole activity such as the central black hole mass, $M_{\rm BH}$, and the accretion rate, $\dot{M}$, as well as the disc–jet coupling.

Until less than ten years ago, quasars and active galactic nuclei, and the supermassive black holes believed to power them, were regarded as exceptional (and extreme) objects. However, beginning with the work of Kormendy & Richstone (1995) and, in particular, Magorrian et al. (1998), the idea that SMBH reside in the nuclei of virtually every galaxy in the nearby universe has become almost commonplace. A sharp picture of the demographics of local SMBH comes from the work of Ho, Filippenko, & Sargent

[1] For the case of stellar mass objects, these signatures are common to most neutron stars, too. In this cases, only dynamical studies can provide a proof of the black hole nature of the source.

© 0000 RAS

(1997b), who have carried out a detailed optical spectroscopic survey of a large number of nearby galaxies. From this work, it was found that between a third and a half of the sample has AGN-like spectra, albeit of low luminosity, (LLAGN; either of the LINER, Seyfert or Transition type; see Ho, Filippenko, & Sargent 1997a), thus confirming that SMBH are not only present in galaxies, but that they are also active (at least as some level). As a matter of fact, follow-up radio surveys of optically selected LLAGN (Ho & Ulvestad 2001; Nagar et al. 2002) have yielded extremely high detection rates, with the radio emission having predominantly a compact core morphology, occasionally accompanied by jet-like features. X-ray studies at arcsecond (or sub-arcsecond) resolution with the *Chandra* X-ray Observatory have also allowed us to firmly pin down the emission properties of the nearby dim galactic nuclei through systematic surveys of LLAGN (Ho et al. 2001; Terashima et al. 2002; Terashima & Wilson 2003). These pieces of information on local, low-luminosity objects nicely complement those on more luminous (and more distant) "classical" AGN (i.e. Seyfert galaxies, QSOs, radio galaxies) and allow us to investigate the dependences of observable properties on black hole mass and accretion rate.

As a matter of fact, alongside the work on black hole demographics, there have been various claims for the existence of a correlation between radio luminosity or radio loudness (a measure of the ratio of radio to bolometric luminosity) and SMBH masses (Franceschini, Vercellone, & Fabian 1998; McLure & Dunlop 2001; Lacy et al. 2001; Nagar et al. 2002; Laor 2000). Comparisons of radio emission from GBH and SMBH has also led to the suggestion that there is a systematic difference in radio loudness between the two classes, SMBH being on average more radio loud (Falcke & Biermann 1996). Furthermore, among X-ray binaries, black holes tend to be more radio loud than neutron stars (Fender & Kuulkers 2001), possibly also indicating a mass dependence of the radio loudness parameter. However, the difficulty of separating the dependence of the radio power output on the accretion rate (due to the lack, or the neglect, of an independent observational indicator of it for SMBH) unavoidably makes the evidence of any such correlation rather weak. Indeed, other authors, using different samples, have recently found no evidence for such correlations (Ho 2002a; Woo & Urry 2002; Oshlack, Webster, & Whitting 2002).

A link between the disc accretion rate and the generation of relativistic radio jets has been suggested by Willott et al. (1999) for radio galaxies and by Ho & Peng (2001) for Seyfert 1 nuclei, on the basis of the strong observed correlations between radio and optical powers. Moreover, by studying a sample of galactic nuclei with measured black hole masses, Ho (2002) found clear evidence of radio loudness being anti-correlated with some estimator of the dimensionless accretion rate. Interestingly, Brinkmann et al. (2000) have also correlated the ROSAT All-Sky Survey and the VLA FIRST catalog, and have shown that there is some degree of correlation between the monochromatic X-ray luminosity at 2 keV and the radio (5 GHz) luminosity for bright AGN and Quasars (for both radio loud and radio quiet sources), while Sambruna et al. (1999) have found a weak correlation between lobe radio power and 2-10 keV luminosity in a sample of radio loud AGN.

The situation is rather different for GBH where the measured black hole masses span a very narrow range (around 10 solar masses). In this case, the observed, rather large, changes in luminosity can only be explained if they are somehow linked to variations in the accretion rate. On this note, recent work has shown that GBHs in the low/hard state (where their spectra are dominated by a power-law X-ray emission with typical bolometric luminosities $L_{\rm bol}/L_{\rm Edd} \lesssim 10^{-2}$) always possess compact radio cores (Fender 2001) the radio luminosity of which is tightly correlated with their X-ray luminosity over more than three orders of magnitude, with $L_{\rm R} \propto L_{\rm X}^{0.7}$ (Gallo, Fender, & Pooley 2002; Gallo, Fender, & Pooley 2003; Corbel et al. 2003). The evidence of such a correlation emphasizes the effects of the dependence of the radio luminosity on the accretion rate and hence the connection between accretion and jet processes. However, an alternative model has been put forward recently, based on the broad band spectral energy distributions of some GBH in the low/hard state, in which the X-ray emission from those objects is produced by optically thin synchrotron radiation emerging from the jet itself (Markoff, Falcke, & Fender 2001). The tightness of the observed correlation between radio and X-ray luminosity, and its slope, seem to support such an idea (Markoff et al. 2003; Corbel et al. 2003).

Finally, we should also note that GBH with bolometric luminosity close to their Eddington limit display a more complicated behavior when observed in the radio band. There is evidence that in the high/soft state (when the spectral energy distribution is dominated by a quasi-thermal component with $kT \sim 1$ keV) continuous jet production is inhibited, while at still higher luminosities (in the so-called very high state) powerful, episodic super-luminal ejection events have been observed (in particular in the prototypical microquasar GRS 1915+105, Mirabel & Rodriguez, 1994). Thus, high luminosity black hole X-ray binaries seem to display a (temporal) dichotomy between radio loud and radio quiet states, reminiscent of that of powerful quasars.

This rapid (albeit somewhat disorderly) progress in the observational studies of black holes of all classes seems to offer the possibility for understanding fundamental scalings of black hole properties with $M_{\rm BH}$ and $\dot{M}$. Accretion disc theory can provide us with the relationships between the observed radiative output (hence X-ray luminosity) and the black hole masses and accretion rates. Unfortunately, theoretical modeling of the relation between jet properties (related to the observed radio luminosity) and the physical parameters of the system ($M_{\rm BH}$, $\dot{M}$) has been hampered by the lack of a clear understanding of the mechanism by which jets are accelerated and collimated. Relating the X-ray and radio properties of a black hole system to only $M_{\rm BH}$ and/or $\dot{M}$ has not been straightforward. However, in a recent paper, Heinz & Sunyaev (2003) have demonstrated that, under the general assumption that the jet formation process is not qualitatively different among SMBH of different mass or between SMBH and GBH, it is in fact possible to derive a universal scaling between the jet (radio) luminosity at a given frequency, L_ν, and both mass and accretion rate. The derived relation is *independent of the jet model* and has scaling indices that depend only on the (observable) spectral slope of the synchrotron emission in the radio band, and on the accretion model (see § 5 below).

Motivated by these findings, the aim of this work is twofold. First, we want to examine (or re-examine) the significance of the correlations between radio and X-ray luminosities with $M_{\rm BH}$ and with each other in a large sample of black holes with measured masses that includes *both* GBH and SMBH. This will be dealt with in the first part of the paper: in §2, we describe the selection criteria and the properties of our sample, while in §3 and §4 we present the results of the correlation analysis and we describe the observational properties of the fundamental plane of black hole activity. Then, in the second part of the paper (§5) we will make use of the model by Heinz & Sunyaev (2003) to relate observed correlation coefficients that define the fundamental plane to theoretically predicted ones. This will allow us to place constraints on the physical properties of the accretion flow from which the jet is launched, and in particular on its radiative efficiency. Section 6 is devoted to a discussion of our findings and of their general implications for our understanding of black hole activity in different regimes. Finally, we summarize our results in §7

2 THE SAMPLE

2.1 Supermassive black holes in galactic nuclei

We have selected from the existing literature a sample of black hole-powered systems with measured masses, the nuclei of which have been observed both at 5 GHz (mostly with arcsecond resolution with the VLA) and in the 2-10 keV band. For future reference we define the dimensionless black hole mass $M = M_{\rm BH}/M_{\odot}$ and accretion rate $\dot{m} \equiv (L_{\rm bol}/\eta)/L_{\rm Edd} = \dot{M}c^2/L_{\rm Edd} \propto \dot{M}/M$, where η is the accretion efficiency.

We first considered the full sample of ~ 40 nearby inactive, or weakly active galaxies with existing nuclear black hole mass measurements from observations of spatially resolved kinematics. To these we have added a comparable number of bright AGNs (and QSOs) with nuclear black hole mass measured from reverberation mapping of their broad line region (a similar sample was compiled by Ho et al. 2002). From this sample we selected all objects which have been observed in both the radio and X-ray bands.

In order to obtain a more statistically representative sample, we also searched the existing literature for both nearby low-luminosity galactic nuclei (Ho et al., 2001; Terashima et al., 2002; Nagar et al., 2002; Terashima & Wilson, 2003) and for relatively bright Seyfert nuclei (either type 1, type 2 or Narrow Line Seyfert 1) and radio galaxies with available radio and X-ray flux measurements. We assign black hole masses to these systems using the observed correlation between black hole masses and stellar velocity dispersion (Gebhardt et al. 2000; Ferrarese & Merritt 2000) [2], mostly using the values of the velocity dispersion provided by the HYPERLEDA catalogue (Simien & Prugniel 2002). We note here that it is beyond the scope of this paper to discuss the different methods (and their qualities) for estimating black hole masses in the nuclei of galaxies, and refer the reader to the comprehensive literature on the subject (see e.g. De Zeeuw, 2003, and references therein).

We do not include in our sample distant quasars, for which the $M-\sigma$ relation cannot be used because of the lack velocity dispersion measurements. In practice, we want to avoid any indirect method for black hole mass estimation that relies on e.g. the continuum optical/UV luminosity (as done by Woo & Urry, 2002, for example).

Relativistically beamed sources (i.e. those whose jet axis points towards our line of sight) are dominated by the boosted jet emission, and cannot be used to test the disc-jet coupling. We therefore excluded from our sample BL Lac objects. Among the Quasars in our sample, only 3C 273, which has an extremely high radio loudness and a blazar-like spectrum, is likely to suffer from strong Doppler boosting of the radio jet. On the other hand, according to the unification scheme, Seyfert 2 nuclei should not be preferentially viewed pole on. For all the other sources (mainly low-luminosity AGN and Seyfert 1), for which the nature of the (relatively faint) radio emission is not well established, we have assumed that the orientation of their jets with respect to line of sight is randomly distributed. A more detailed discussion of the possible incidence of relativistic beaming as a selection effect will be presented in §6.2.

[2] We use here the relationship $M = 1.3 \times 10^8 (\sigma/200 {\rm km\,s^{-1}})^{4.58}$, as derived in Ferrarese (2002). See however Tremaine et al. (2002) for a thorough statistical discussion of the different scalings that have been claimed for the $M-\sigma$ relation.

2.2 Galactic black hole sources

The Galactic X-ray binaries included in our sample have been selected to have (a) simultaneous X-ray and radio observations, or *RXTE* All-Sky-Monitor (ASM) X-ray data in conjunction with radio fluxes available from the literature, and (b) publicly available *RXTE*-ASM X-ray and Green-Bank Interferometer (GBI) radio lightcurves (from which we estimated the 5 GHz fluxes by interpolating between the 2.25 GHz and the 8.3 GHz channels).

We treated the GBI and ASM data of each object in the following way: we first re-gridded the ASM X-ray lightcurve to the radio lightcurve, and then sorted the data into bins of ascending X-ray flux. This procedure assumes that individual bins are not correlated and can thus be re-ordered and rebinned to improve statistics. Rebinning the data in time intervals does not change the results significantly, but reduces the dynamic range in X-ray flux. In this sense, X-ray-flux-ordered binning produces a better representation of the scatter in this variable. Since the GBI becomes noise dominated below about 15 mJy, we conservatively chose to consider data at or below this value as upper limits and split the sample into detection and upper limits before binning. ASM fluxes were converted to $2-10$ keV luminosities using the a conversion factor of 3.2×10^{-10} $[{\rm erg\,s^{-1}\,cm^{-2}}]/[{\rm cts\,s^{-1}}]$ (Grimm, Gilfanov, & Sunyaev 2002), which assumes a crab-like source spectrum.

Black hole masses for GBH are derived from stellar kinematics and we use the value provided in the literature. For the microquasar LS 5039, no mass estimate is available, and we assumed $M_{\rm BH} = 10\,M_{\odot}$.

2.3 Global properties of the sample

Our final sample (Table 1) comprises 149 entries, of which 99 are individual SMBH systems. The remaining 50 correspond to the observations of 8 different GBH at various luminosity levels. Out of these 8 sources, 5 are so-called X-ray transients (Cyg X-3, GRO J1655-40, GRS 1915+105, XTE J1118+480 and XTE J1859+226) and 3 persistent sources (Cyg X-1, GX 339-4 and LS 5039). The SMBH sample includes 14 Quasars; 19 Seyfert galaxies of type 1 (in this class we include all the Seyfert spectrally classified as types 1 to 1.9); 32 Seyfert 2 galaxies; 7 Narrow Line Seyfert 1 galaxies (NS1); 11 Low-Ionization Nuclear Emission line Regions (LINERS) of type 1.9; 13 LINERS of type 2 and 2 LINER/HII Transition nuclei. Separating mass estimators into direct ones (stellar kinematics, maser emission, gas kinematics and, to a lesser extent, reverberation mapping) and indirect ones (all those that infer a measure of the central black hole mass from the observed $M-\sigma$ relation), we can assess possible biases introduced in our sample by the different mass measurement techniques. 55 masses are measured indirectly (4 Sy1, 4 NS1, 30 Sy2, 15 LINERs and the two transition objects) and 44 directly (all the 14 QSOs, 15 Sy1, 2 Sy2, 3 NS1, 8 LINERs plus Sgr A* and M 32).

For the radio and X-ray luminosities taken from the literature, we have assumed $H_0 = 75$ km s^{-1} Mpc^{-1}, correcting the quoted values when necessary. When available, we have included information on the radio spectral properties of the sources. In Table 1 we have marked all the sources with flat radio spectrum ($\alpha_{\rm R} < 0.4$, where $\alpha_{\rm R}$ is the radio spectral index $\alpha \equiv -\partial \ln L_\nu / \partial \ln \nu$ evaluated at the frequency ν =5 GHz) with flag (F). All the sources

Table 1. Radio and X-ray properties of black holes with measured masses

Object (1)	D(Mpc) (2)	SC (3)	Log $L_{\rm R}$ (4)	$\alpha_{\rm R}$ (5)	Ref (6)	Log $L_{\rm X}$ (7)	Ref (8)	Log M (9)	Method (10)	Ref (11)
Ark 564	99.0	NS1	38.59	U	1	43.74	2	6.5	$\mathrm{I}_{[OIII]}$	3
Cyg A	224	S2/L2	41.43	F	11	44.22	59	9.4	G	58
Fairall 9	199.8	S1	<37.68	U	4	44.14	5,6	7.91	R	21
IC 1459	29.2	L2	39.71	F	4,53	40.66†	9	9	S	10
IC 4296 (PKS 1333-33)	188	L1.9	39.68	S	11	41.20	12	9.1	I_σ	13
IC 4329A	65.5	S1	38.94	U	4	43.72	5	6.69	R	21
Mrk 3	52.0	S2	39.86	S	14,51	42.7	14,15	8.81	I_σ	16
Mrk 78	149	S2	39.86	S	14,53	<44	14	7.92	I_σ	16
Mrk 279	127	S1.5	38.78	S	4,49	43.72	5	7.62	R	21
Mrk 335	107	NS1	38.27	F	4,49	43.30	2,17	6.79	R	21
Mrk 348	60.0	S2	39.70	F	14,52	42.85	14	7.17	I_σ	16
Mrk 478	316	NS1	38.75	U	18	43.87	2	7.30	$\mathrm{I}_{[\mathrm{OIII}]}$	3
Mrk 507	216	NS1	38.78	U	1	42.97	2	7.10	$\mathrm{I}_{[\mathrm{OIII}]}$	3
Mrk 509	144	NS1	38.30§	S	19,56	44.00	20	7.86	R	4
Mrk 573	69.2	S2	38.22	S	14,49	<43.00	14	7.25	I_σ	16
Mrk 590	109	S1.2	38.70	S	4,49	43.58	57	7.23	R	21
Mrk 766	51.7	NS1	38.32	S	1,22	42.90	2,6	6.64	$\mathrm{I}_{[\mathrm{OIII}]}$	3
Mrk 1066	48.4	S2	38.68	S	14,53	<41.85	14	6.93	I_σ	16
NGC 221 (M 32)	0.810	-	<33.3	U	67	35.97	67	6.40	S	68
NGC 315	66.2	L1.9	40.41	F	23	41.68	24	9.10	I_σ	16
NGC 1052	19.6	L1.9	39.86	S	25	41.57	24	8.29	I_σ	16
NGC 1068	14.4	S1.9	39.12	S	4,27	41.00	15	7.20	M	4
NGC 1275	70.1	S2	41.74	F	14,27	43.40	32,34	8.64	I_σ	16
NGC 1365	21.8	S1.8	38.80	S	53	40.60	24	7.66	I_σ	26
NGC 1386	11.6	S2	36.70	U	53	40.64	24	7.20	I_σ	16
NGC 1667	61.2	S2	37.34	S	14,27	40.05	15	7.93	I_σ	16
NGC 2110	31.2	S2	38.99	F	14,53	42.60	14,15	8.41	I_σ	16
NGC 2273	28.4	S2	37.83	S	27	41.40	15,24	7.27	I_σ	16
NGC 2787	7.5	L1.9	37.22	F	4,29	38.40	24,28	7.59	G	10
NGC 2841	12.0	L2	36.00	F	29	38.26	28	8.42	I_σ	30
NGC 2992	30.8	S2	38.64	U	14	42.10	14,15	7.75	I_σ	16
NGC 3031 (M81)	3.9	S1.5	36.82	F	4,29	39.90	24,28	7.79	S	4
NGC 3079	20.4	S2	38.39	F	27,50	40.20	15	7.65	I_σ	26
NGC 3147	40.9	S2	38.01	F	27,31	41.61	15,31	8.79	I_σ	26
NGC 3169	16.5	L2	37.19	F	31,54	41.35	31	7.91	I_σ	33
NGC 3226	15.4	L1.9	37.20	F	31,54	40.74	31	8.23	I_σ	34
NGC 3227	20.6	S1.5	37.94	S	4,27	41.99	5	7.59	R	21
NGC 3362	111	S2	38.47	S	14,49	<43.6	14	6.68	I_σ	16
NGC 3516	38.9	S1	37.98	S	4,27	43.20	5,6	7.36	R	4
NGC 3627	6.6	S2	35.45	F	29	<37.6	28	7.26	I_σ	30
NGC 3675	12.8	T2	<35.99	U	29	<37.99	28	7.11	I_σ	30
NGC 3998	14.1	L1.9	37.98	S	4,53	41.66	24	8.75	S	4
NGC 4051	17.0	NS1	37.30	S	4,27	41.50	5,6	6.11	R	21
NGC 4117	124	S2	35.70	S	14	39.4‡	45	6.74	I_σ	16
NGC 4143	17.0	L1.9	37.16	F	29,31	40.03	31	8.32	I_σ	34
NGC 4151	20.3	S1.5	38.49	S	4,27	42.83	5,6	7.17	R	21
NGC 4203	14.1	L1.9	36.79	F	29,31	40.23	28,31	7.90	I_σ	30
NGC 4258	7.3	S1.9	35.94	F	4,29	40.52	35	7.60	M	4
NGC 4261 (3C 270)	29.6	L2	39.21	U	11	41.17	24	8.72	G	4
NGC 4278	9.7	L1.9	37.91	F	29,31	39.96	31	9.20	S	60
NGC 4321	16.8	T2	<36.17	U	29	<38.59	28	6.80	I_σ	30
NGC 4374 (M84)	18.4	L2	38.81	F	4,29	40.34	24	9.20	G	4
NGC 4388	16.8	S2	36.95	S	27	42.76	15	6.80	I_σ	26
NGC 4395	3.6	S1.5	35.56	S	4,27	39.50	36	<5.04	S	4
NGC 4450	16.8	L1.9	36.53	F	29	40.34	24	7.30	I_σ	26
NGC 4457	17.4	L2	<35.70	U	29	39.97	24	6.86	I_σ	26
NGC 4472	18.8	S2	36.69	S	27,29	<38.80	37	8.80	I_σ	38
NGC 4486 (M87)	16.1	L2	39.78	F	4,29	40.55	39	9.48	G	4
NGC 4494	9.7	L2	<35.65	U	29	38.86	28	7.65	I_σ	30

Table 1 – *continued*

NGC 4501	16.8	S2	36.20	S	27	40.28	14	7.90	I_σ	26
NGC 4548	16.8	L2	36.30	F	29	39.79	31	7.40	I_σ	26
NGC 4565	9.7	S1.9	36.15	F	29,31	39.56	31	7.70	I_σ	26
NGC 4579	16.8	S1.9	37.65	F	29,31	41.14	28,31	7.85	I_σ	26
NGC 4594 (M104)	9.8	L2	37.84	F	4,53	40.70	15	9.04	S	4
NGC 4636	17.0	L1.9	36.40	U	29	<38.43	37	7.90	I_σ	38
NGC 4725	12.4	S2	<35.90	U	29	39.16	28	7.49	I_σ	30
NGC 4736	4.3	L2	34.80	F	29	39.62	24	7.30	I_σ	26
NGC 5033	18.7	S1.5	36.79	S	27	41.00	24,28	7.30	I_σ	30
NGC 5194	7.7	S2	35.50	S	27	39.80	15	6.90	I_σ	16
NGC 5252	92.3	S2	38.96	S	14,49	42.97	14	8.12	I_σ	16
NGC 5273	21.3	S2	36.22	F	14,24	<42.0	14	6.37	I_σ	16
NGC 5347	31.2	S2	37.10	F	14,55	40.0[‡]	45	6.70	I_σ	16
NGC 5548	70.2	S1.5	38.58	S	4,27	43.55	5	8.03	R	21
NGC 5929	33.2	S2	38.30	S	14,49	40.7[‡]	45	7.22	I_σ	16
NGC 6166	116	S2	39.95	S	40	40.56	41	9.19	I_σ	26
NGC 6251	94.8	S2	40.93	S	4,53	42.15	15	8.73	G	4
NGC 6500	40.0	L2	38.90	F	31,54	40.11	31	8.28	I_σ	30
NGC 7469	66.6	S1	38.38	S	4,49	43.31	42	6.81	R	21
NGC 7672	53.2	S2	37.25	S	14,55	43.37	14	6.80	I_σ	16
NGC 7682	68.0	S2	38.88	S	14,49	<43.2	14	7.25	I_σ	16
NGC 7743	24.4	S2	36.99	S	27	39.71	24	6.47	I_σ	16
PG 0026+129	627	Q	40.17	U	4	44.44	43	7.73	R	21
PG 0052+251	690	Q	39.42	U	4	44.66	44	8.34	R	21
PG 0804+761	430	Q	39.41	U	4	44.26	43	8.28	R	21
PG 0844+349	268	Q	38.12	U	4	43.29	43	7.34	R	21
PG 0953+414	1118	Q	40.14	U	4	44.50	43	8.26	R	21
PG 1211+143	362	Q	41.08	U	4	43.61	43	7.61	R	21
PG 1226+023 (3C273)	705	Q	44.03	F	4,56	45.70	44	8.74	R	21
PG 1229+204	268	Q	38.45	U	4	44.29	44	7.88	R	21
PG 1307+085	690	Q	38.98	U	4	44.51	44	8.44	R	21
PG 1411+442	380	Q	38.71	U	4	43.53	43	7.90	R	21
PG 1426+015	366	Q	38.98	U	4	43.89	44	8.67	R	21
PG 1613+658	565	Q	39.75	F	4,56	44.34	44	8.38	R	21
PG 1700+518	1406	Q	40.92	S	4,53	<43.20	43	7.78	R	21
PG 2130+099	255	Q	38.89	S	4,56	43.55	44	8.16	R	21
3C120	138	S1	41.55	F	11,53	43.95	11	7.36	R	21
3C 390.3	241	S1	41.09	S	11	44.00	11	8.53	R	21
UGC 6100	116	S2	38.50	U	14	<43.6	14	7.72	I_σ	16
Sgr A*	0.008	-	32.50	F	62	33.34	63	6.41	S	64
Cyg X-1	0.0021	GBH	<29.44	F	61	36.44	61	1.06	S	69
Cyg X-1	0.0021	GBH	<29.45	F	61	36.57	61	1.06	S	69
Cyg X-1	0.0021	GBH	29.63	F	61	36.48	61	1.06	S	69
Cyg X-1	0.0021	GBH	29.65	F	61	36.57	61	1.06	S	69
Cyg X-1	0.0021	GBH	29.66	F	61	36.64	61	1.06	S	69
Cyg X-1	0.0021	GBH	29.24	F	72	36.58	61	1.06	S	69
Cyg X-1	0.0021	GBH	29.30	F	72	36.65	61	1.06	S	69
Cyg X-1	0.0021	GBH	29.18	F	72	36.66	61	1.06	S	69
Cyg X-3	0.009	GBH	<30.64	F	61	36.94	61	1.00	S	70
Cyg X-3	0.009	GBH	31.62	F	61	37.19	61	1.00	S	70
Cyg X-3	0.009	GBH	31.85	F	61	37.41	61	1.00	S	70
Cyg X-3	0.009	GBH	32.17	F	61	37.60	61	1.00	S	70
Cyg X-3	0.009	GBH	32.43	U	61	37.88	61	1.0	S	70
GRO J1655-40	0.0032	GBH	<29.76	F	61	36.64	61	0.85	S	65
GRO J1655-40	0.0032	GBH	<29.69	F	61	37.55	61	0.85	S	65
GRO J1655-40	0.0032	GBH	29.94	F	61	35.27	61	0.85	S	65
GRS 1915+105	0.0125	GBH	<30.89	F	61	38.17	61	1.20	S	65
GRS 1915+105	0.0125	GBH	<30.89	F	61	38.47	61	1.20	S	65
GRS 1915+105	0.0125	GBH	<30.89	F	61	38.73	61	1.20	S	66
GRS 1915+105	0.0125	GBH	31.60	F	61	38.25	61	1.20	S	66
GRS 1915+105	0.0125	GBH	31.76	F	61	38.40	61	1.20	S	66
GRS 1915+105	0.0125	GBH	31.76	F	61	38.65	61	1.20	S	66

Table 1 – *continued*

GX 339-4	0.004	GBH	29.91	F	7	36.48	7	1.00	S	8
GX 339-4	0.004	GBH	29.87	F	7	36.42	7	1.00	S	8
GX 339-4	0.004	GBH	29.89	F	7	36.40	7	1.00	S	8
GX 339-4	0.004	GBH	29.62	F	7	36.12	7	1.00	S	8
GX 339-4	0.004	GBH	29.71	F	7	36.12	7	1.00	S	8
GX 339-4	0.004	GBH	29.66	F	7	36.14	7	1.00	S	8
GX 339-4	0.004	GBH	29.45	F	7	35.81	7	1.00	S	8
GX 339-4	0.004	GBH	29.11	F	7	35.32	7	1.00	S	8
GX 339-4	0.004	GBH	28.34	F	7	34.21	7	1.00	S	8
GX 339-4	0.004	GBH	28.02	F	7	33.91	7	1.00	S	8
GX 339-4	0.004	GBH	28.38	F	7	33.84	7	1.00	S	8
GX 339-4	0.004	GBH	28.49	F	7	34.01	7	1.00	S	8
GX 339-4	0.004	GBH	<27.51	F	7	<33.34	7	1.00	S	8
GX 339-4	0.004	GBH	<27.25	F	7	33.19	7	1.00	S	8
LS 5039	0.003	GBH	29.80	S	61	35.62	61	1.00	-	-
LS 5039	0.003	GBH	30.09	S	61	35.45	61	1.00	-	-
LS 5039	0.003	GBH	30.07	S	61	35.67	61	1.00	-	-
LS 5039	0.003	GBH	30.09	S	61	35.81	61	1.00	-	-
LS 5039	0.003	GBH	30.08	S	61	35.96	61	1.00	-	-
XTE J1118+480	0.0018	GBH	<28.98	F	46	35.43	47	1.00	S	48
XTE J1118+480	0.0018	GBH	28.92	F	71	35.46	61	1.00	S	48
XTE J1118+480	0.0018	GBH	28.92	F	71	35.57	61	1.00	S	48
XTE J1118+480	0.0018	GBH	28.92	F	71	35.56	61	1.00	S	48
XTE J1118+480	0.0018	GBH	28.92	F	71	35.47	61	1.00	S	48
XTE J1118+480	0.0018	GBH	28.92	F	71	35.45	61	1.00	S	48
XTE J1859+226	0.011	GBH	<29.24	F	61	36.58	61	>0.88	S	71
XTE J1859+226	0.011	GBH	<29.30	F	61	36.65	61	>0.88	S	71
XTE J1859+226	0.011	GBH	29.18	F	61	36.66	61	>0.88	S	71

NOTE: Comments: † $L_{\rm X}$ calculated from the known luminosity in the 0.3-8 keV band and the observed spectral index; ‡ $L_{\rm X}$ calculated from the GIS count rate, assuming $\Gamma = 2$ and $Log(N_{\rm H}) = 22.5$; § $L_{\rm 5Ghz}$ extrapolated from observations at 8 GHz. Col.(1): Name of the object. Col. (2): Distance in Megaparsecs (for $H_0 = 75$ km s^{-1} Mpc^{-1}). Col. (3): Spectral Class; GBH: Galactic black hole; L: LINER; S: Seyfert; NS1: Narrow Line Seyfert 1; T: Transition object (LINER/H II); Q: Quasar. Col. (4) Logarithm of nuclear luminosity at 5GHz. Col. (5): Radio spectral index $\alpha_{\rm R}$ (where $F_\nu = \nu^{-\alpha_{\rm R}}$); F: flat spectrum ($\alpha_{\rm R} < 0.4$); S: steep spectrum ($\alpha_{\rm R} > 0.4$); U: undetermined. Col. (7) Logarithm of the intrinsic rest-frame luminosity in the 2-10 keV band. Col. (9) Logarithm of the black hole mass. Col. (10) Mass measurement method; S: stellar kinematics; G: gas kinematics; M: maser kinematics; R: reverberation mapping; $I_{\rm [OIII]}$: inferred from the mass-[OIII] line-width correlation; I_σ: inferred from the mass-velocity dispersion correlation.

REFERENCES: (1) Ulvestad, Antonucci & Goodrich (1995); (2) Leighly (1999); (3) Wang & Lu (2001); (4) Ho (2002); (5) Weaver, Gelbord & Yaqoob (2001); (6) Nandra et al. (1997); (7) Corbel et al. (2003); (8) Hynes et al. (2003); (9) Fabbiano et al. (2003); (10) Tremaine et al. (2002); (11) Sambruna, Eracleous & Mushotzky (1999); (12) Pellegrini et al. (2003); (13) Saglia et al. (1993); (14) Polletta et al. (1996); (15) Bassani et al. (1999); (16) Woo & Urry (2002); (17) Gondoin et al. (2002); (18) Zhou & Wang (2002); (19) Thean et al. (2001); (20) Pounds et al. (2001); (21) Kaspi et al. (2000); (22) Ho & Peng (2001); (23) Gregory & Condon (1991); (24) Terashima et al. (2002); (25) Griffith et al. (1995); (26) Simien & Prugniel (2002) and HYPERLEDA Catalogue: http://www-obs.univ-lyon1.fr/hypercat/; (27) Ho & Ulvestad (2001); (28) Ho et al. (2001); (29) Nagar et al. (2002); (30) Barth, Ho & Sargent (2002); (31) Terashima & Wilson (2003); (32) Allen et al. (2001); (33) Hereudeau & Simien (1998); (34) Churazov et al. (2003); (35) Fabbiano et al. (1992); (36) Shih et al. (2003); (37) Loewenstein et al. (2001); (38) Merritt & Ferrarese (2001); (39) Di Matteo et al. (2003); (40) Giovannini et al. (1998); (41) Di Matteo et al. (2001); (42) De Rosa, Fabian & Piro (2002); (43) George et al. (2000); (44) Lawson & Turner (1997); (45) Moran et al. (2001); (46) Dhawan et al. (2000); (47) Frontera et al. (2001); (48) Wagner et al. (2001); (49) Rush, Malkan & Edelson (1996); (50) Becker, White & Edwards (1991); (51) Kojoan et al. (1980); (52) White, Giommi & Angelini (2000); (53) Véron-Cetty & Véron (2001); (54) Falcke et al. (2001); (55) Ulvestad & Wilson (1989); (56) Falcke, Malkan & Biermann (1995); (57) Turner & Pounds (1989); (58) Tadhunter et al. (2003); (59) Young et al. (2002); (60) Magorrian et al. (1998); (61) This work; (62) Melia & Falcke (2001); (63) Baganoff et al. (2001); (64) Schödel et al. (2002); (65) Orosz & Bailyn (1997); (66) Greiner, Cuby & McCaughrean (2001); (67) Ho, Terashima & Ulvestad (2003); (68) Verolme et al. (2002); (69) Dolan (1992); (70) Hanson, Still & Fender (2000); (71) Filippenko & Chornock (2001); (72) Stirling et al. (2001), (73) Fender et al. (2001); .

with $\alpha_{\rm R} > 0.4$ are instead classified as steep spectrum (S), while those for which the radio spectral index couldn't be determined are marked with a (U). Overall, we have 77 flat spectrum sources (32 SMBH and 45 GBH, respectively); 43 steep spectrum sources (38 and 5) and 29 for which the spectral slope is undetermined (all SMBH).

In Figure 1 we show the distributions of black hole masses, radio and X-ray luminosities and that of the ratio of their X-ray to the Eddington luminosity, $L_{\rm X}/L_{\rm Edd} = L_{2-10{\rm keV}}/1.3 \times 10^{38} M$. It is worth emphasizing that the shape of those distributions reflects more the nature of our selection procedure rather than the global intrinsic properties of accreting black holes. For example, a precise measurement of the central black hole mass is a prerequisite for a given source to be included in the sample. As recently discussed by De Zeeuw (2003), not all mass ranges are equally well probed by the different methods, and this should introduce a strong selection effect in our sample. Similarly, because BH masses are more easily measured in the nuclei of nearby galaxies, our sample is biased against the most luminous quasars. This should be taken into account when examining, for example, the $L_{\rm X}/L_{\rm Edd}$ distribution of the black holes in our sample.

In Figure 2 we show the radio luminosity versus the black

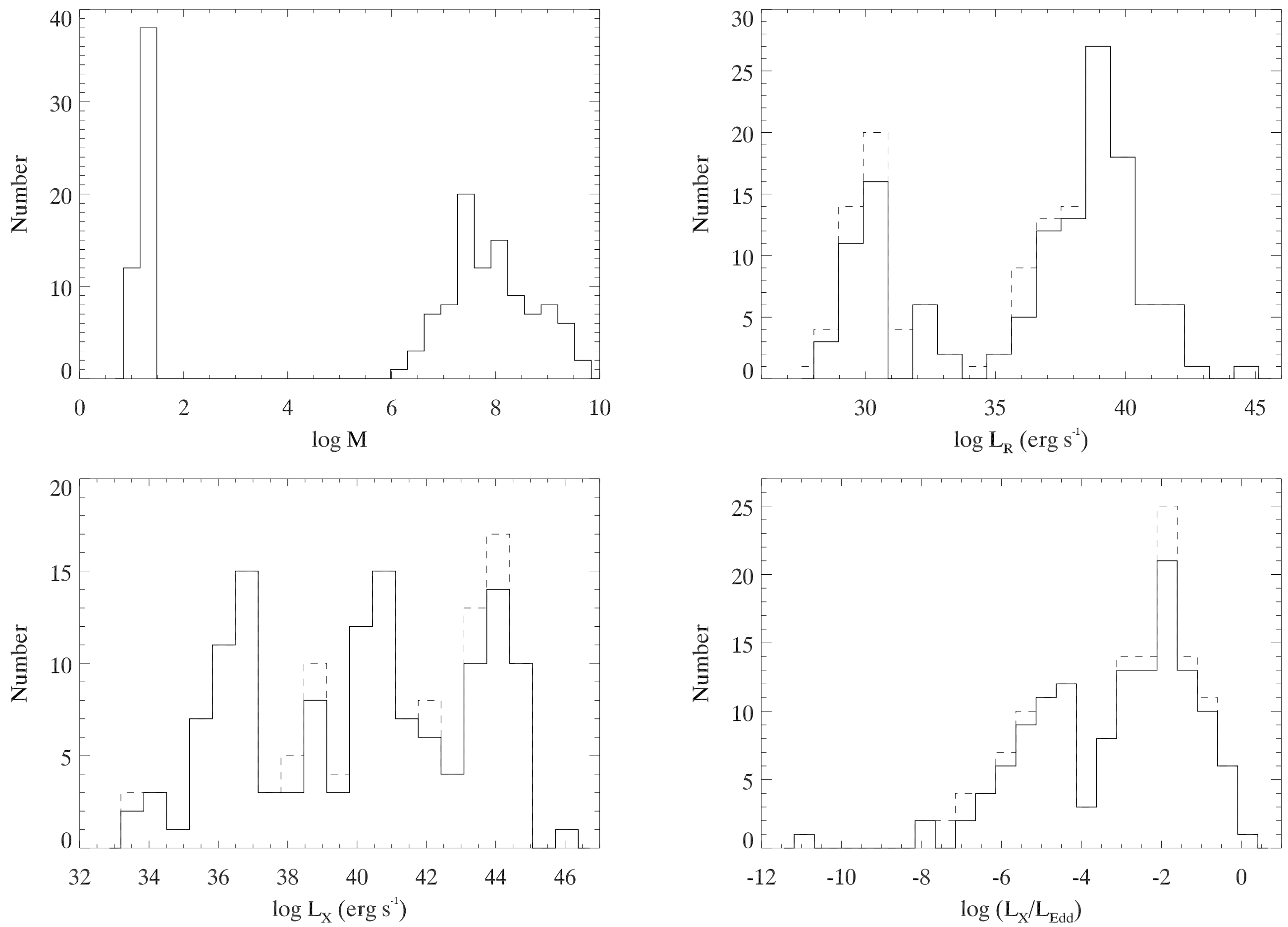

Figure 1. Distribution of black hole masses (top left panel), 5 GHz radio luminosity ($L_{\rm R}$, top right panel), 2-10 keV X-ray luminosity ($L_{\rm X}$, bottom right panel) and of the ratio $L_{\rm X}/L_{\rm Edd}$. Solid histograms denote detected sources, dashed ones are for upper limits.

hole mass for objects of different spectral classes. Panel (a) shows the whole sample, while panel (b) concentrates on the SMBH only. Overplotted are some of the linear regression fits discussed in the recent literature (see §3 for details).

Finally, Figure 3 shows the core radio luminosity versus the nuclear X-ray luminosity in the 2-10 keV band (left panel) and versus the ratio of the X-ray nuclear luminosity to the Eddington luminosity (right panel). We represent objects in different mass bins with different colors to highlight a possible segregation of different mass bins in the $L_{\rm R} - L_{\rm X}$ plane.

In the next section we present a more quantitative statistical analysis of the correlations among $L_{\rm R}$, $L_{\rm X}$, and M.

3 CORRELATION ANALYSIS

Luminosity-luminosity correlations have to be tested for possible spurious effects introduced by their common dependence on the distance. Such tests can be done by performing a partial correlation analysis, taking distance as the third variable. Here we choose the so-called partial Kendall's τ correlation test, proposed by Akritas & Seibert (1996) in the case of censored data sets. Applying this test to our data, we find that the $L_{\rm R} - L_{\rm X}$ correlation is strong: the probability of the null hypothesis (i.e. that there is no correlation) is less that 10^{-10} for the whole sample and $\sim 1.12 \times 10^{-4}$ for the SMBH only (see Table 2).

However, it is apparent from Fig. 3 that, when the data points are grouped into mass bins, objects in different bins tend to lie on parallel tracks. Such a behavior can be seen both in the $L_{\rm R} - L_{\rm X}$ plane (panel a), and, perhaps even more clearly, in the $L_{\rm R} - L_{\rm X}/M$ plane (panel b). The presence of a mass segregation suggests that the radio luminosity of an object likely depends both on its X-ray luminosity and on its mass. In order to assess this hypothesis we once again use partial correlation analysis, now taking $L_{\rm R}$ (or $L_{\rm X}$) as the dependent variable and testing its partial correlation with $L_{\rm X}$ ($L_{\rm R}$) where we take M as the third variable. In addition, we also look for a partial correlation between $L_{\rm R}$ ($L_{\rm X}$) with mass itself, by taking $L_{\rm X}$ ($L_{\rm R}$) as the third variable. In so doing we can effectively discriminate between intrinsic and spurious correlations among the three quantities.

The results of such tests (see Table 2) show that the radio luminosity is strongly correlated with both black hole mass and X-ray luminosity ($P_{\rm null} < 1 \times 10^{-10}$ for the whole data set), while in turn, the X-ray luminosity correlates with both mass and radio luminosity only if we include both GBH and SMBH ($P_{\rm null} \simeq 4.68 \times 10^{-5}$). These results imply that any regression fit used to find correlations between any two variables that does not account for the dependence on the third one (as, for example trying to find the dependence of $L_{\rm R}$ on M without accounting for the dependence on $L_{\rm X}$), inevitably leads to an incorrect estimate of the correlation coefficients.

If, in any case, we compute the correlation coefficients between any two of these variables[3] to allow a comparison with earlier works, we find that $\log L_{\rm R}^{\rm SMBH} = (29.54 \pm 1.60) + (1.23 \pm 0.20)\log M$, with a very large scatter (standard deviation $\sigma_{\rm RM}^{\rm SMBH} = 1.65$). Including GBH, we find $\log L_{\rm R}^{\rm all} = (28.75 \pm 0.18) + (1.20 \pm 0.04)\log M$ (standard deviation $\sigma_{\rm RM}^{\rm all} = 1.51$), which is indeed very similar to what found by Nagar et al. (2002), but very different from what was proposed by Franceschini et al. (1998), based on a much smaller sample (as shown by the different linear regression fits plotted in Figure 2).

We emphasize, however, that the partial correlation analysis presented so far and summarized in Table 2, implies that a far better representation of the mutual dependencies of $L_{\rm R}$, $L_{\rm X}$ and M (and the one that minimizes the scatter) should be searched for with multivariate linear regression tests, that allow simultaneous fitting over the 3-dimensional space defined by the three variables.

3.1 Finding the multivariate correlation coefficients

The standard multivariate regression formalism does not treat dependent and independent variables symmetrically (see, e.g., Fasano & Vio 1988). In other words, if a linear regression analysis yields a linear regression coefficient b for the dependence of y on x, it does not necessarily yield a coefficient b^{-1} for the dependence of x on y. Closely related to this is the fact that standard χ^2 statistics, for which errors are only associated with the dependent variable, artificially reduce the estimate of the correlation coefficient in the presence of intrinsic scatter in the independent variable. The net result of these shortcomings is that χ^2 distributions over the fitting parameter space are not fair representations of the confidence in the resulting best fit.

In order to alleviate these shortcomings, we extend the statistical approach used by the "Nukers" group (Gebhardt et al. 2000; Tremaine et al. 2002) to obtain an unbiased estimator of the best fit regression coefficients in multivariate problems. This approach uses a modified chisquare estimator, called the merit function (Fasano & Vio 1988; Press et al. 1992; Tremaine et al. 2002), defined by

$$\hat{\chi}^2 = \sum_i \frac{(y_i - a - \sum_j b_j x_{ij})^2}{\sigma_{y_i}^2 + \sum_j (b_j \sigma_{x_{ij}})^2} \tag{1}$$

where y_i is the dependent variable, x_{ij} are the independent variables and σ_{y_i} and $\sigma_{x_{ij}}$ the associated error estimates, a is the zero intercept, and $\mathbf{b}$ are the linear regression coefficients, which are to be found. The argument of the sum in eq. (1) is a measure of the projected distance of the data point $P_i = (x_{ij}, y_i)$ to the regression hyperplane given by the equation $y = a + \sum_j b_j x_j$, measured in the χ^2 space around point P_i. In other words, the argument of the sum in eq. (1) counts the number of χ^2 intervals between P_i and the regression hyperplane. Because eq. (1) is nonlinear in b_j, it is no longer possible to minimize $\hat{\chi}^2$ analytically. However, for a set of parameters $\mathbf{b}$, we can still find the optimal value $a_{\rm min}(\mathbf{b})$ for which $\hat{\chi}^2$ is minimized as

$$a_{\rm min}(\mathbf{b}) = \frac{\sum_i \frac{(y - \sum_j b_j x_{ij})}{\sigma_{y_i}^2 + \sum_j (b_j \sigma_{x_{ij}})^2}}{\sum_i \left(\sigma_{y_i}^2 + \sum_j (b_j \sigma_{x_{ij}})^2\right)^{-1}} \tag{2}$$

Finding the best fit parameters is then a simple minimization problem which can be treated with standard numerical minimization routines. Because our analysis is restricted to a bivariate problem in this paper, it is possible to use a graphical solution in the form of 2-D $\hat{\chi}^2$ contour plots.

Unfortunately, such a technique cannot handle censored data. However, it is easy to verify that the incidence of the censored data points in our sample on the estimate of the linear regression coefficient is small compared to the intrinsic scatter in the data. In order to do so, we have performed standard linear regression fit using specific techniques that are able to handle censored data, as implemented in the ASURV package (Isobe, Feigelson, & Nelson 1986), on the whole data sample both with and without the upper limits. The differences in the resulting multivariate linear correlation coefficients in the two cases are much smaller than the estimated errors.

In the limit of $\sigma_{y_i} \gg \sigma_{x_{ij}}$, the merit function in eq. (1) recovers the traditional χ^2 estimator. This implies that the usefulness of eq. (1) is limited to cases where the estimated errors are an accurate representation of the true intrinsic uncertainty, including intrinsic scatter. Artificially large errors in one variable will introduce an asymmetry similar to that intrinsic to the traditional regression formalism. At face value, the errors in our sample are dominated by the uncertainties in the mass measurements. However, because we are using a sample of predominantly low redshift low luminosity AGN, error in the distance measurements can be large due to peculiar velocities, which leads to large errors in the luminosity measurements as well. For Galactic sources, distance estimates typically carry even larger uncertainties. Worse yet, the resulting errors in $L_{\rm X}$ and $L_{\rm R}$ will be correlated. As a first step, we therefore decided to follow the Nuker approach and assume isotropic uncertainties $\sigma_{M_{\rm i}} = \sigma_{L_{\rm X},i} = \sigma_{L_{\rm R},i}$ in all three variables and re-normalize these errors to produce a minimum reduced $\hat{\chi}^2_{\rm red} = \hat{\chi}^2/n_{\rm dof}$ of unity.

4 RESULTS

We fit the data with the function

$$\log L_{\rm R} = \xi_{\rm RX} \log L_{\rm X} + \xi_{{\rm R}M} \log M + b_{\rm R}, \tag{3}$$

or, alternatively with its reciprocal

$$\log L_{\rm X} = \xi_{\rm XR} \log L_{\rm R} + \xi_{{\rm X}M} \log M + b_{\rm X}, \tag{4}$$

where we have used the merit function to estimate the best fit linear regression coefficients. Because the regression technique we adopt is symmetric[4], eqs. (3) and (4) contain the same amount of information.

Our final results of the multivariate regression analysis are shown in the form of χ^2 contour plots (using eq. (1) as a χ^2 estimator) in the $(\xi_{\rm RM}, \xi_{\rm RX})$ parameter space in Fig. 5. The top panel shows the results of the multivariate fit performed on the entire

[3] We use a the linear regression method by parametric EM algorithm (that deals with censored data) as implemented in the ASURV package (Isobe, Feigelson, & Nelson 1986)

[4] We verified that the standard regression technique is instead not symmetric: for the same fitting function (3), the best fit parameters are $\xi_{\rm RX} = 0.57$ and $\xi_{\rm RM} = 0.77$, while by fitting eq. (4) we obtain $\xi_{\rm XR} = 1.05$ and $\xi_{\rm XM} = -0.49$, instead of the expected $\xi_{\rm XR} = 1/\xi_{\rm RX} = 1.75$ and $\xi_{\rm XM} = -\xi_{\rm RM}/\xi_{\rm RX} = -1.35$.

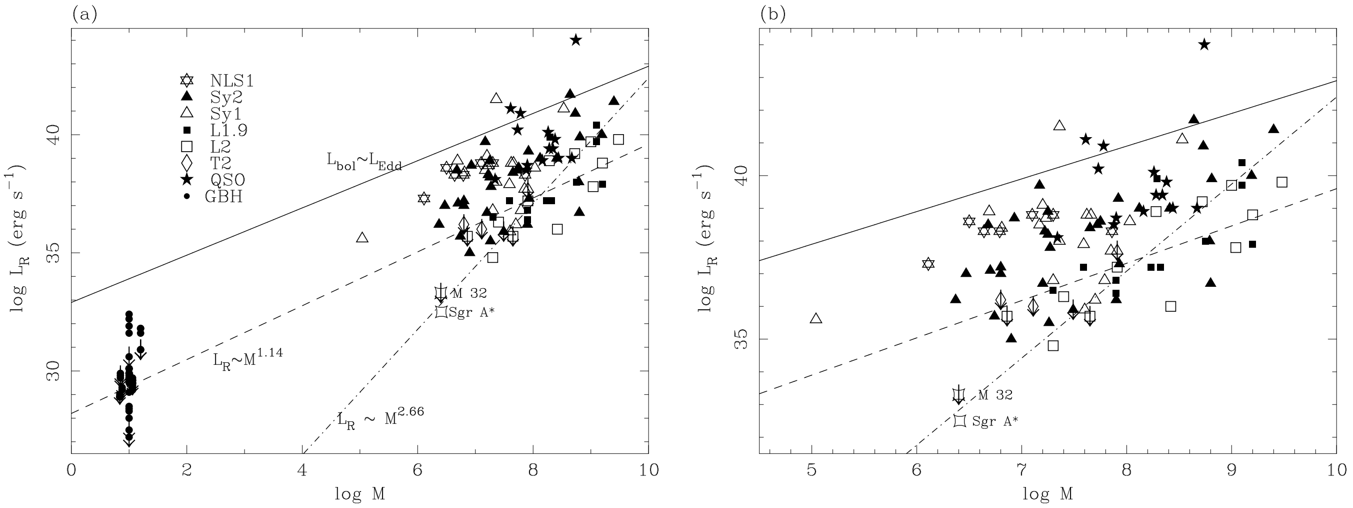

Figure 2. Radio core luminosity at 5 GHz versus black hole mass. Upper limits are marked with arrows. Panel (a) shows the whole sample, including GBH (black filled circles) and SMBH, with different symbols indicating objects belonging to different spectral classes. The right panel (b) is a blow up of the SMBH sample. The dot-dashed line gives the regression fit proposed by Franceschini et al. (1998), the dashed line that proposed by Nagar et al. (2002), both obtained using different samples of SMBH only. The thick solid upper line gives the maximum core radio power as calculated by Ho (2001) for sources accreting at the Eddington rate. Although a correlation analysis of our sample would give results similar to those obtained by Nagar et al. (2002), as we discuss in the text, *none* of the above relations reflects the real physical scaling of radio power and black hole mass.

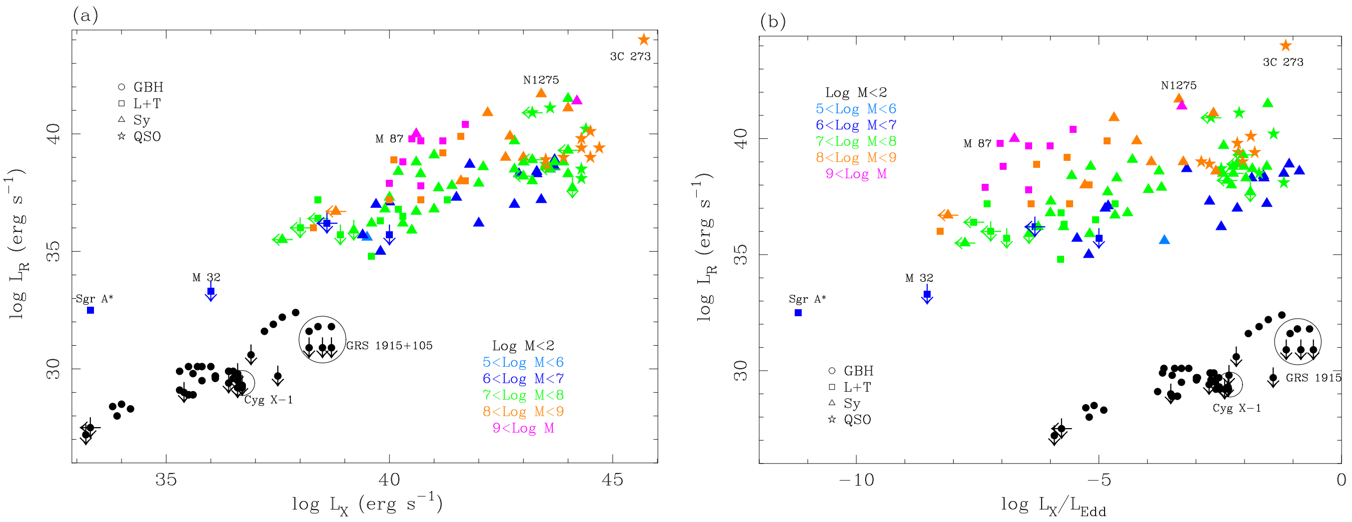

Figure 3. Radio core luminosity at 5 GHz versus X-ray luminosity in the 2-10 keV band (a) for the whole sample. Different colors correspond to different mass bins, while different symbols correspond to different classes of objects. In panel (b) we plot the same radio core luminosity at 5GHz vs. the ratio L_X/L_{Edd} of X-ray to Eddington luminosity. The color-coding of the different mass bins makes the mass segregation more evident.

data set. We obtain $\xi_{RX} = 0.60 \pm 0.11$, $\xi_{RM} = 0.78^{+0.11}_{-0.09}$, and $b_R = 7.33^{+4.05}_{-4.07}$ (all the errors are one sigma confidence), with a dispersion $\sigma_R = 0.88$, or, cast in the form of eq. (3):

$$\log L_R = (0.60^{+0.11}_{-0.11}) \log L_X + (0.78^{+0.11}_{-0.09}) \log M + 7.33^{+4.05}_{-4.07} \quad (5)$$

The value we obtain for the ξ_{RX} correlation coefficient is consistent, within the errors, with that found in GBH ($\xi_{RX} \approx 0.7$) by Gallo et al. (2003). This also means that individual GBH sources for which the correlation between radio and X-ray luminosities is well established (GX 339-4 and V404 Cyg) do indeed follow the same global trend defined by black holes of all masses included in our sample.

Our data set provides fairly tight constraints on the values of the correlation coefficients ξ_{ij} $(i, j = \mathrm{R}, \mathrm{X}, \mathrm{M})$. This in turn implies that in the 3-dimensional space $(\log L_R, \log L_X, \log M)$ the sources are distributed preferentially on a plane, that we call hereafter the "fundamental plane" describing black hole activity. Figure 4 shows an edge-on view of the plane.

The other two panels of Fig. 5 show the constraints on the two correlation coefficients obtained with the regression analysis on different subsamples assembled according to the spectral properties in the radio band. For flat spectrum radio sources we obtain $\xi_{RX,f} = 0.76 \pm 0.13$, $\xi_{RM,f} = 0.71 \pm 0.10$, and $b_{R,f} = 1.31^{+4.85}_{-5.07}$, with a dispersion $\sigma_{R,f} = 0.81$, smaller than that of the whole data set. The difference in the coefficient for the $L_R - L_X$ correlation with respect to the whole sample result may be due to a larger incidence of GBH in the flat spectrum subsample, which seem to have a slightly larger measured value of ξ_{RX} (Gallo, Fender, & Pooley

Table 2. Results of Correlation analysis

Variables			Subsample					Correlation		
X (1)	Y (2)	Z (3)	Objects (4)	N (5)	N^X_{ul} (6)	N^Y_{ul} (7)	N^Z_{ul} (8)	τ (9)	σ (10)	Pnull (11)
Log $L_{\rm R}$	Log $L_{\rm X}$	Log D	All Objects	149	20	14	0	0.255	0.0414	7.3×10^{-10}
Log $L_{\rm R}$	Log $L_{\rm X}$	Log D	SMBH only	99	7	13	0	0.200	0.0518	1.12×10^{-4}
Log $L_{\rm R}$	Log $L_{\rm X}$	M	All Objects	149	20	14	1	0.448	0.0495	$< 1 \times 10^{-10}$
Log $L_{\rm R}$	Log $L_{\rm X}$	M	SMBH only	99	7	13	1	0.450	0.0523	$< 1 \times 10^{-10}$
Log $L_{\rm R}$	M	Log $L_{\rm X}$	All Objects	149	20	1	14	0.432	0.0469	$< 1 \times 10^{-10}$
Log $L_{\rm R}$	M	Log $L_{\rm X}$	SMBH only	99	7	1	13	0.310	0.0547	1.45×10^{-8}
Log $L_{\rm X}$	M	Log $L_{\rm R}$	All Objects	149	14	1	20	0.184	0.0452	4.68×10^{-5}
Log $L_{\rm X}$	M	Log $L_{\rm R}$	SMBH only	99	13	1	7	-0.022	0.052	0.672

NOTE: Col. (1): Variable X. Col. (2): Variable Y. Col (3): Variable Z. Correlation between variables X and Y is studied, taking into account the mutual correlation of X nd Y with Z. Col. (4): subsample. Col. (5): Number of objects in the subsample. Col. (6)-(8): Number of upper limits in X, Y and Z. Col. (9)-(11): Results of partial correlation analysis, giving the partial Kendall's τ correlation coefficient, the square root of the calculated variance σ, and the associated probability $P_{\rm null}$ for accepting the null hypothesis that there is no correlation between X and Y.

2002); the constraints on the other coefficient, $\xi_{\rm RM}$ are almost as good as for the entire data set, and in very good agreement with it.

On the other hand, in our steep spectrum sources subsample, only one GBH is included (LS 5039), and this results in a much larger uncertainty, in particular on the radio luminosity-mass correlation coefficient: ($\xi_{\rm RX,s} = 0.41^{+0.16}_{-0.18}$, $\xi_{\rm RM,s} = 0.94^{+0.21}_{-0.19}$, $b_{\rm R,s} = 14.08^{+5.92}_{-6.31}$ with dispersion $\sigma_{\rm R,s} = 0.87$).

5 PHYSICAL INTERPRETATION OF THE FUNDAMENTAL PLANE RELATION

As stated in the introduction, a correlation between X-ray and radio emission is expected if there is a fundamental connection between accretion flows and jet activity. Thus, at a qualitative level, the existence of the fundamental plane found in §4 is not surprising. However, on a quantitative level, the presence of such a plane and the measurement of the correlation coefficients associated with it provide powerful probes of accretion physics and of the inner jet.

In the following section we will therefore lay out an avenue of how to use the fundamental plane relation to constrain accretion and jet physics. In order to do this, we shall first turn to a discussion of the theory of the radio and of the X-ray emission by the jet–disc system. We will first make use of the scale invariant assumption about the disc–jet coupling (Heinz & Sunyaev 2003) to derive the expected scalings of the radio luminosity with black hole mass and accretion rates. Then, we will show how these theoretically predicted correlation coefficients translate into observable ones between black hole mass and X-ray luminosity ($\xi_{\rm RM}, \xi_{\rm RX}$) for different models of the X-ray emission. By comparing these theoretical predictions to the observed values from eq. (5) we will then discuss the constraints we can put on the models themselves.

5.1 Synchrotron emission from scale invariant jets

It was recently shown by Heinz & Sunyaev (2003) that the dependence of radio luminosity $L_{\rm R}$ on black hole mass M and dimensionless accretion rate $\dot{m}$ can be cast into a model independent form *if the underlying jet physics is scale invariant*. In this case, all the model dependent uncertainties can be absorbed into the observable spectral index α. The relationships between $L_{\rm R}$ and M and between $L_{\rm R}$ and $\dot{m}$ depend only on the boundary conditions at the base of the jet, set by the conditions in the accretion flow feeding the jet. We will briefly review their argument (the interested reader is encouraged to consult Heinz & Sunyaev, 2003, for more details) before comparing their predictions to the correlations derived in the previous section.

The nature and conditions in the inner disc are most likely governed by only a few parameters (M, $\dot{m}$, and possibly the black hole spin a). The fundamental scale imposed on the problem is the gravitational radius of the black hole, $R_{\rm g} = GM_{\rm BH}/c^2$. Jet formation occurs in the innermost regions of accretion discs, thus it is natural that jet formation, too, is primarily governed by these three parameters only[5].

Then, we make the *ansatz* that jet structure and dynamics are (at least approximately) invariant under changes of $R_{\rm g} \propto M$ and $\dot{m}$. In other words, taking a jet produced by a black hole of mass M_1, scaling its dimensions by a factor of M_2/M_1 we should obtain a jet around a black hole of mass M_2.

This proposed invariance can be cast into a simple mathematical form. Any quantity f needed to calculate the synchrotron emission from jets can be decomposed into a structure function $\psi_f(\mathbf{R}/R_{\rm g}, a)$, which describes the spatial variation of f along the jet, and which depends on M only through $\mathbf{R}/R_{\rm g}$, and a normalization $\phi_f(M, \dot{m}, a)$, which is set by the boundary conditions at the base of the jet (thus, by accretion disc physics):

$$f(\mathbf{R}, M, \dot{m}, a) = \phi_f(M, \dot{m}, a) \cdot \psi_f(\mathbf{R}/R_{\rm g}, a) \qquad (6)$$

The quantities necessary for calculating the jet synchrotron emission are the magnetic field strength B, the jet diameter $D_{\rm jet}$, and the normalization C of the electron power-law distribution $dn_{\rm e}/d\gamma = C\gamma^{-p}$ (typically, the spectral index of the particle distribution is $p \sim 2-3$). For example, according to the prescription (6), the magnetic field should follow $B = \phi_B(M, \dot{m}, a) \cdot \psi_B(\mathbf{R}/R_{\rm g}, a)$, where $\phi_B = B_0 = B(R_0)$ is the value of the field at the base of the jet R_0. As a geometric quantity, the jet diameter D should be directly proportional to the characteristic scale $R_{\rm g}$ such that $\phi_D = D_0 = D(R_0) \propto R_{\rm G} \propto M$. Scale invariance also

[5] The influence of a and the associated second scale of the problem, the light cylinder radius, on jet formation is unclear at this point. We will henceforth keep a fixed and assume that variations in a will only introduce a scatter in any relation derived below which is independent of M and $\dot{m}$.

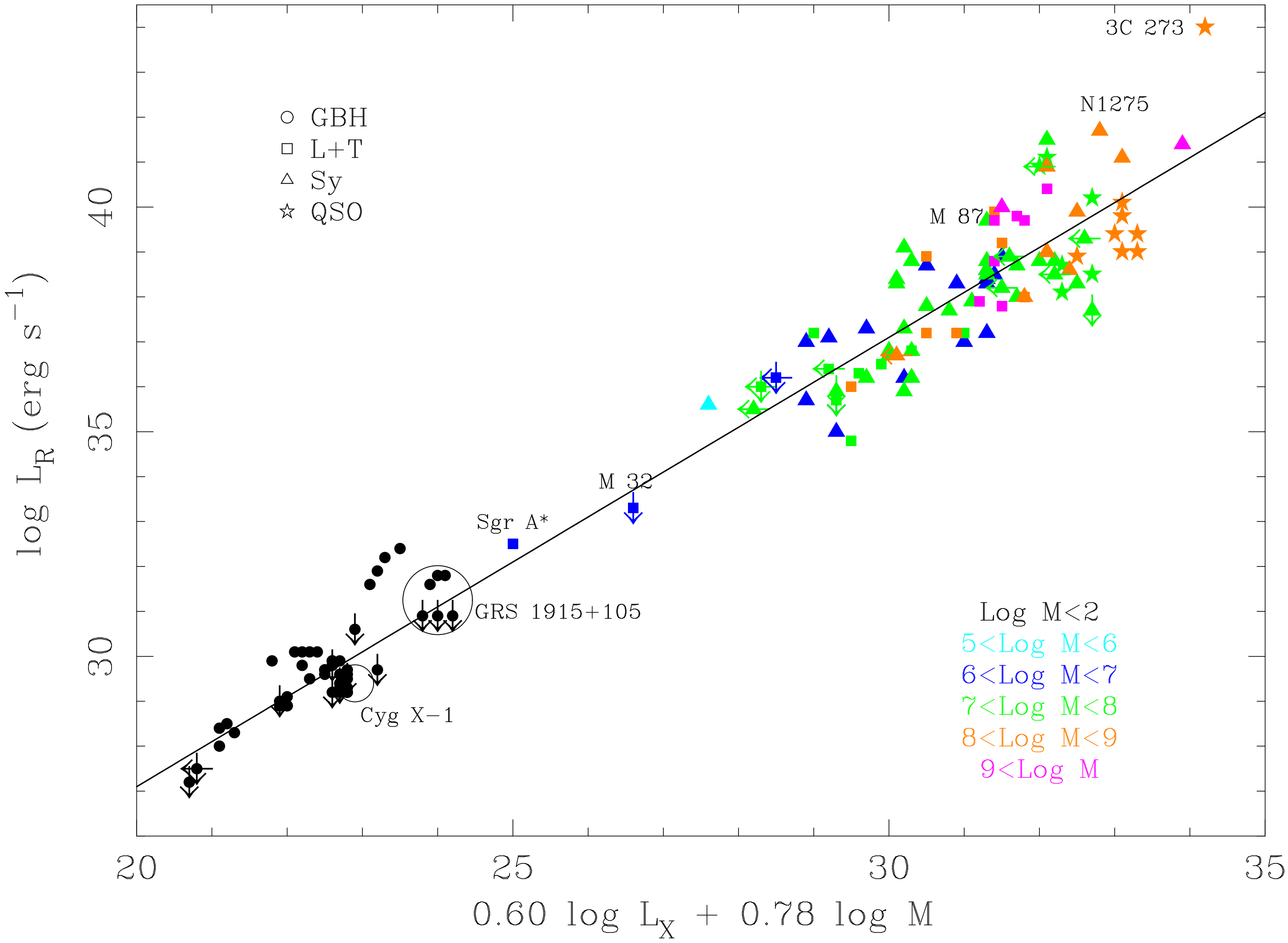

Figure 4. The edge-on view of the "fundamental plane of black hole activity". The solid line shows the best fitting function (5).

implies that dynamical time scales are proportional to $R_{\rm g}/c \propto M$, and thus that characteristic velocities are scale invariant.

Using the standard formulae for synchrotron emission (Rybicki & Lightman 1979), Heinz & Sunyaev (2003) showed that the synchrotron luminosity L_ν at a given frequency ν emitted by the jet must then depend non-linearly on M and $\dot{m}$, following

$$\frac{\partial \ln (L_\nu)}{\partial \ln (M)} = \frac{2p+13+2\alpha}{p+4} + \frac{\partial \ln (\phi_B)}{\partial \ln (M)} \left(\frac{2p+3+\alpha p+2\alpha}{p+4}\right) + \frac{\partial \ln (\phi_C)}{\partial \ln (M)} \left(\frac{5+2\alpha}{p+4}\right) \equiv \xi_M \quad (7)$$

and

$$\frac{\partial \ln (L_\nu)}{\partial \ln (\dot{m})} = \frac{\partial \ln (\phi_B)}{\partial \ln (\dot{m})} \left(\frac{2p+3+\alpha(p+2)}{p+4}\right) + \frac{\partial \ln (\phi_C)}{\partial \ln (\dot{m})} \left(\frac{5+2\alpha}{p+4}\right) \equiv \xi_{\dot{m}} \quad (8)$$

where α is the spectral index at frequency ν.

Note that the model dependent structure functions $\psi_f(\mathbf{R}/R_{\rm g}, a)$ scale out from these expressions. Only the spectral indices (α and p) and the boundary conditions ϕ_B and ϕ_C for the magnetic field B and the electron power-law distribution normalization C, respectively, remain. α and p are observables: the electron spectral index p can be deduced from the optically thin synchrotron spectral index at high frequencies. The functions ϕ_B and ϕ_C, on the other hand, need to be provided by accretion disc theory. It is reasonable to assume that the relativistic particle pressure at the injection radius is a fixed fraction (i.e., independent of M and $\dot{m}$) of the total pressure at injection, $\phi_C \propto \phi_B^2$. This leaves ϕ_B as the only model dependent parameter of the theory. Given a prescription for ϕ_B, we can predict how the synchrotron luminosity of jets should scale with M and $\dot{m}$.

Since ξ_M and $\xi_{\dot{m}}$ are constants, we have in general (with $L_\nu = L_{5\,{\rm GHz}} = L_{\rm R}$)

$$\log L_{\rm R} = \xi_M \log M + \xi_{\dot{m}} \log \dot{m} + K_1, \quad (9)$$

where K_1 is a normalization constant[6]. Variations in other parameters, such as the viewing angle or the black hole spin, will only introduce a scatter in this relationship that is *independent* of M and $\dot{m}$.

Because the expressions for ξ_M and $\xi_{\dot{m}}$ do not depend on the shape functions ψ_f, they are independent of the model details. Any

[6] We note here that for flat spectrum jets with $\alpha_{\rm R} \sim 0$, the canonical value of $p \sim 2$, and $\phi_B^2 \propto M^{-1}\dot{m}$, the dependence of $L_{\rm R}$ on M and $\dot{m}$ follows $L_{\rm R} \propto (M\dot{m})^{17/12} = \dot{M}^{17/12}$, as had been found by Falcke & Biermann (1996) for the specific case of the "canonical conical" (Blandford & Königl 1979) jet model.

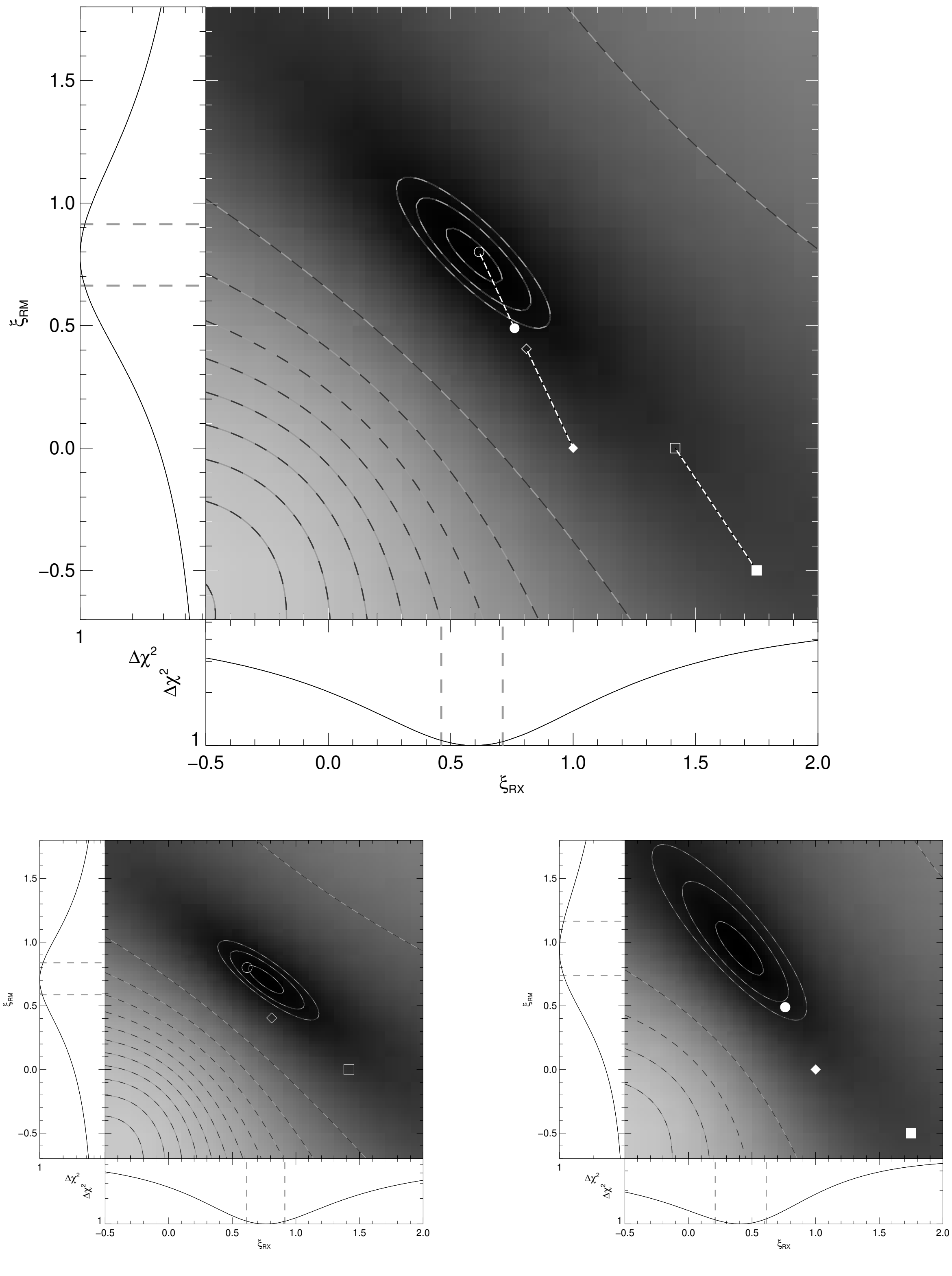

Figure 5. Shaded areas show the χ^2 density distribution, and dashed lines the χ^2 contours for the observed correlation coefficients $\xi_{\rm RM}$ and $\xi_{\rm RX}$. The inner 3 contours show the formal 1,2 and 3 sigma confidence levels, the remaining contours further out show levels of $\Delta\chi^2_{\rm red} = 10$. Shown are the results for: the entire data set (upper panel), the flat spectrum sources (lower left panel), the steep spectrum sources (lower right panel). Overplotted on each panel are the theoretically predicted values of the correlation coefficients where circles, diamonds and squares represent the ADAF, jet and standard disc models respectively. Empty symbols show the values for $\alpha_{\rm R} = 0$ and filled ones for $\alpha_{\rm R} = 0.5$. The lines connecting the points represent the tracks of $\xi_{\rm RX}$ and $\xi_{\rm RM}$ traced out by variation of $\alpha_{\rm R}$.

scale-invariant jet model that reproduces the observed radio spectral index $\alpha_{\rm R}$ *must* satisfy eqs. (7) and (8). This implies that (a) measurements of ξ_M and $\xi_{\dot m}$ *cannot* be used to constrain the functions ψ_f, i.e., they cannot be used to distinguish between different jet models but that (b) measurements of ξ_M and $\xi_{\dot m}$ *can* be used to place constraints on the boundary conditions at the base of the jet ϕ_f, or in other words on the accretion disc model.

While the black hole mass M is observable (see above), the accretion rate $\dot m$ can only be inferred through radiation in other bands, where the emission is dominated by the accretion disc. Thus, in addition to a prescription of the boundary conditions ϕ_f through accretion disc theory, we must also provide a relation between the accretion disc luminosity (or $L_{\rm X}$) and $\dot m$ in order to model the observed $L_{\rm R}$-$\dot m$ correlation. We must therefore discuss the different possible sources of the X-ray emission. We will start with those models that describe X-ray emission as produced by an accretion flow of some kind.

5.2 Accretion flow origin of X-ray radiation

For the accretion powered X-ray luminosity we can write, in analogy to eq. (9):

$$\log L_{\rm X} = \log M + q \log \dot m + K_2 \qquad (10)$$

where K_2 is a normalization constant. The efficiency coefficient q need not be constant, though the linear correlation analysis from §3 is limited to this case.

Using eqs. (7-9) together with eq. (10), we obtain the following general expression for the *observable* correlation coefficients as defined in eqs. (3) and (4):

$$\begin{aligned}\xi_{{\rm R}M} &= \frac{2p+13+2\alpha_{\rm R}}{p+4} + \frac{\partial \ln \phi_B}{\partial \ln M}\left(\frac{2p+13+\alpha_{\rm R}p+6\alpha_{\rm R}}{p+4}\right)\\ &- \frac{\partial \ln \phi_B}{\partial \ln \dot m}\left(\frac{2p+13+\alpha_{\rm R}p+6\alpha_{\rm R}}{q(p+4)}\right)\\ \xi_{\rm RX} &= \frac{\partial \ln \phi_B}{\partial \ln \dot m}\left(\frac{2p+13+\alpha_{\rm R}p+6\alpha_{\rm R}}{q(p+4)}\right). \qquad (11)\end{aligned}$$

Different accretion models imply different values of q, and different scalings of the magnetic energy density at the base of the jet ϕ_B with M and $\dot m$, resulting in different values of $\partial \ln \phi_B / \partial \ln M$ and $\partial \ln \phi_B / \partial \ln \dot m$. In the next two sections we calculate the expected scalings for radiatively efficient and inefficient flows (the results of the calculations are summarized in Table 3). For the case of radiatively efficient accretion, we will consider the X-ray emission to be produced by a standard, geometrically thin and optically thick disc coupled with a hot corona. In the case of radiatively inefficient accretion flows, for the sake of clarity we will describe a detailed spectral modeling in the framework of a pure advective disk (ADAF). Currently this is the simplest existing dynamical model of a radiatively inefficient flow from which we can derive detailed spectral energy distributions. However, one should keep in mind that radiatively inefficient flows may be significantly modified by convection or outflows (see below). We do not, however, expect the arguments laid out below to be significantly modified in such cases.

As a result of our calculations, we will show how the physical properties of radiatively inefficient and efficient discs do indeed imply very different scalings for the observed X-ray luminosity with the accretion rate $\dot m$.

5.2.1 *Radiatively efficient flows*

In the standard Shakura-Sunyaev disc model (Shakura & Sunyaev 1973) accretion occurs via an optically-thick and geometrically thin disc. The effective optical depth in the disc is very high and photons are close to thermal equilibrium with electrons. The emission results in multi-color ($T \propto \dot m^{1/4} M^{-1/4} r^{-3/4}$) blackbody spectrum. This component is thought to explain the "blue bump" in AGN and the soft X-ray emission in GBH. However, the standard model does not predict the power-law X-ray emission observed in all sub-Eddington accreting black holes. In fact, the emission in the 2-10 keV band we are considering here is completely dominated by the power-law spectral component for SMBH and for GBH in the low/hard state.

It is generally accepted that this hard X-ray power-law emission is produced by inverse Compton scattering of the soft, blackbody disc photons on a population of hot electrons that surround the cooler disc in the innermost region of the accretion flow (the so-called *corona*) In these models a fraction $f_{\rm c}$ of the gravitational power is dissipated in the corona (and eventually emerges as X-ray radiation). The X-ray luminosity can then be written as $L_{\rm X} \sim f_{\rm c} \dot m L_{\rm Edd} \propto f_{\rm c} \dot m M$, and the coronal magnetic energy density follows $B^2 \propto \dot m f_{\rm c}/M$ (e.g.; Haardt & Maraschi 1991; Di Matteo, Celotti & Fabian 1999; Merloni & Fabian 2002). $L_{\rm X}$ should therefore scale linearly with $\dot m$, as long as the fraction of power dissipated into the corona $f_{\rm c}$ does not change with the accretion rate. Note, however, that we expect some scatter in any such a relation due to intrinsic changes in the coronal plasma optical depth and temperature that may have some dependence on the accretion rate.

Merloni & Fabian (2002) and Merloni (2003) have shown how it is possible to derive coupled equations for the accretion disc–corona systems under very simple assumptions about the nature of the turbulent magnetic viscosity inside the disc. The main property of their self-consistent coupled treatment is that $f_{\rm c}$ is indeed constant when gas pressure dominates in the disc, so for accretion rates $\dot m \lesssim 0.016(\alpha_{\rm v} M)^{-1/8}(1-0.84\alpha_{\rm v}^2)^{-9/8}$ (with $\alpha_{\rm v}$ viscosity parameter) we should expect $q=1$. On the other hand, $f_{\rm c} \propto \dot m^{-1/2}$ in the radiation pressure dominated parts of the disc, and $q = 1/2$ (see Table 3). It is worth noting that q and $\partial \phi_B / \partial \dot m$ enter eq. (11) in such a way that the correlation coefficients $\xi_{\rm RM}$ and $\xi_{\rm RX}$ are identical for the gas and radiation pressure dominated disc cases.

5.2.2 *Radiatively inefficient flows*

The standard solution we have discussed in the previous section is not a unique solution for the accretion flow equations at low accretion rates. In recent years, much work has been devoted to the detailed study of low radiative efficiency accretion and in particular to the so called Advection Dominated Accretion Flows (ADAF) solutions (Narayan & Yi 1994; Narayan & Yi 1995; Abramowicz et al. 1995; Narayan, Mahadevan, & Quataert 1998). The latter usually refers to the optically–thin ADAF branch which is established only for accretion rates lower than a critical value $\dot m < \dot m_{\rm crit} \sim \alpha_{\rm v}^2$ (Rees et al. 1982). However, both from the theoretical point of view (Narayan, Igumenschev, & Abramowicz 2000) and from numerical simulations (Igumenschev & Abramowicz 2000; Hawley & Balbus 2002), it has been shown that that radiatively inefficient flows are prone to strong convective instabilities and/or powerful outflows which alter the nature of the solutions significantly. Despite the extensive theoretical efforts, however, the relative importance of convection and outflow for adiabatic flows is still a matter of significant debate (Balbus & Hawley 2002; Narayan et al. 2002) and no strong observational discriminant has yet been found.

From our point of view, it is important to understand how the value of the magnetic field in such flow scales with M and $\dot{m}$, and to have a detailed model for their radiative output, in order to predict the scaling of the X-ray emission with these parameters. From general arguments, we expect any mechanically cooled flow to obey $\phi_B^2 \propto M^{-1}\dot{m}$ (Heinz & Sunyaev 2003). On the other hand, the exact value of q can only be determined once a detailed assessment of the radiative processes that give rise to observed luminosity is made. This is what we discuss in the following.

A hot accretion flow around a stellar mass (supermassive) black hole radiates mostly in the optical (radio) to X–ray bands. In the optical (radio) band, the emission results from synchrotron radiation. At higher energies, and up to the X-ray band, the emission is produced by bremsstrahlung processes for low accretion rates and inverse Compton scattering of the soft synchrotron photons or blackbody photons from the disc in the outer regions when the accretion rate approaches the critical value (Narayan, Barrett, & McClintock 1998). The predicted spectrum from an ADAF depends (weakly) on the ratio of the gas to magnetic pressure β, the viscosity parameter $\alpha_{\rm v}$, and the fraction of the turbulent energy in the plasma which heats the electrons, δ. Here, we fix $\alpha_{\rm v} = 0.1$, $\beta = 10$, and take $\delta = 0.3$.

The top panel of Figure 6 shows the spectra of ADAFs (plus outer thin disc for $\dot{m} \sim \dot{m}_{crit}$) for ten accretion rate values starting from $\dot{m} = 10^{-6}$ up to $\dot{m} \sim \dot{m}_{crit} \sim 10^{-2}$. The bottom panel shows the relationship between the $2-10$ keV luminosity, $L_{\rm X}$, and the accretion rate, $\dot{m}$ (for $M = 10$). For the chosen values of the parameters $\alpha_{\rm v}$, β and δ, the dependence of the 2-10 keV luminosity on $\dot{m}$ is roughly given by (see also Beckert & Duschl 2002, for a similar calculation):

$$L_{X,2-10\rm keV} \propto \begin{cases} \dot{m}^{3.4}, & \dot{m} \lesssim 10^{-4} \\ \dot{m}^{1.6}, & 10^{-4} \lesssim \dot{m} \lesssim 5\times10^{-3} \\ \dot{m}^{2}, & 5\times10^{-3} \lesssim \dot{m} \lesssim 2\times10^{-2} \end{cases} \quad (12)$$

The full band spectra shown in Figure 6 with the two vertical lines indicating the $2-10$ keV energy band illustrate the origin for the various dependences shown in equation (12). For $\dot{m} \lesssim 10^{-4}$ the integrated $2-10$ keV emission includes both the first order Comptonized component, which drops off at around few keV, and bremsstrahlung which dominates the emission at higher energies. At higher accretion rates the first (or higher) order Compton scattering of softer photons always dominate the $2-10$ keV emission (see Figure 6, top panel). At these higher rates the optical depth increases and cooling becomes overall more efficient.

This can also been seen in bottom panel of Figure 6, where we also plot (dashed line) the electron temperature at $r = 3$ as a function of $\dot{m}$. The temperature is nearly constant for $\dot{m} \lesssim 10^{-4}$; in this regime the viscous heating is virtually fully balanced by advection. At $\dot{m} \gtrsim 10^{-4}$ cooling processes become more important and the temperature decreases. The overall change in the dependences in eq. (12) reflects this behavior.

However, it is important to keep in mind that the exact dependences in this narrow band will also depend on the microphysical parameters that we choose for the model. For instance, variations in the electron heating parameter, δ will result in changes in the Comptonization spectra. Therefore, in order to compare theoretical predictions with the observed data, the intrinsic scatter of which does not allow us to put tight constraints on the different emission regimes, we fit the $L_{\rm X} - \dot{m}$ relation over the whole range of $\dot{m}$ and obtain a single power-law, $L_{\rm X} \propto \dot{m}^{2.3}$ (i.e. $q = 2.3$, as shown by the solid line in the middle panel of Figure 6). We also calculate the relation between $L_{2-10\,\rm keV}$, versus the black hole mass, M for the models and, as expected, the relation is very close to linear with $L_{\rm X} \propto M^{0.97}$. Overall the scalings derived from our specific computation of a specific ADAF model are consistent with the expected behaviour of the more general class of radiatively inefficient, mechanically cooled accretion flows. In fact, we note here that if the flow is modified by convection or outflows, we expect the X-ray spectrum to be dominated by bremsstrahlung emission (Quataert & Narayan 1999; Di Matteo et al. 1999), for which we expect $q = 2$.

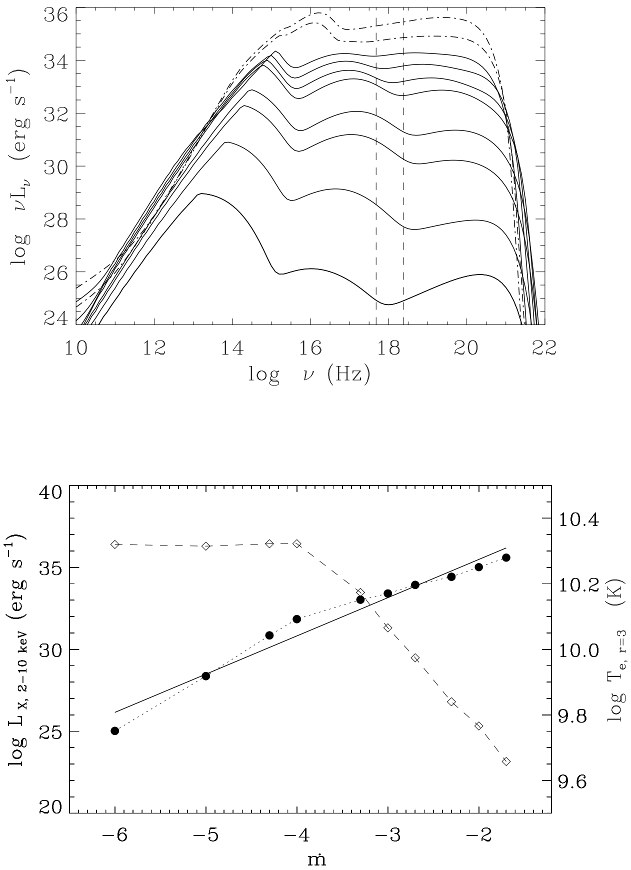

Figure 6. Predictions from ADAF models for $\dot{m} = 10^{-6}, 10^{-5}, 5^{-5}, 10^{-4}, 5\times10^{-4}, 10^{-3}, 2\times10^{-3}, 5\times10^{-3}, 10^{-2}$. The top panel shows the broad band spectral energy distributions for a fixed $M = 10$, with the vertical dashed lines enclosing the $2-10$ keV spectral energy band. For the top two models (dot-dashed lines) we also plot the multicolor blackbody from an outer thin disc with an inner edge at $r = 40$. In the bottom panel: the solid dots joined by the dotted line show the integrated $2-10$ keV X-ray luminosity and the open symbols joined by dashed lines and the flow electron temperature at $r = 3$ versus the accretion rate $\dot{m}$. The solid line is a linear fit to the $2-10$ keV luminosity over the whole of the $\dot{m}$ with slope 2.3.

5.3 Jet origin of X-ray radiation

The presence of both high energy electrons and radio/optical radiation implies that the inner jet must emit inverse Compton X-rays, contributing to the overall X-ray spectrum at some level. How-

Table 3. Scaling indices of the X-ray luminosity and of the magnetic field as functions of the physical parameters $\dot{m}$ and M for different accretion flow models.

accretion model	q	$\frac{\partial \ln \phi_B}{\partial \ln M}$	$\frac{\partial \ln \phi_B}{\partial \ln \dot{m}}$
disc/corona, gas	1	-1/2	1/2
disc/corona, rad	1/2	-1/2	1/4
ADAF	2.3	-1/2	1/2
brehms. emission only	2	-1/2	1/2

ever, under suitable conditions even the synchrotron component will reach X-ray energies. Especially in the presence of relativistic beaming, synchrotron emission could actually be responsible for the bulk of the X-rays. It is therefore useful to discuss the radio-X-ray-mass correlation expected for the synchrotron X-ray scenario (Markoff, Falcke, & Fender 2001).

While at low frequencies the effects of synchrotron self-absorption lead to the flat spectrum typically observed in core dominated sources, at high frequencies the jet becomes optically thin to synchrotron self-absorption, following the well know optically thin power-law with X-ray spectral index $\alpha_{\rm X} = (p-1)/2$.

Because X-rays and radio emission now originate from the same source, it is straightforward to derive the relation between the two components. The correlation coefficients ξ_M and $\xi_{\dot{m}}$ for the optically thick radio emission are still given by eqs. (7) and (8), while for the optically thin X-ray emission we can simply substitute $\alpha_{\rm X} = (p-1)/2$ in those expressions. Finally, we can eliminate log $\dot{m}$ from eq. (9) in favor of log $L_{\rm X}$ and arrive at the desired expressions for the correlation coefficients:

$$\begin{aligned}\tilde{\xi}_{\rm RX} &= \frac{2(2p+13+\alpha_{\rm R}p+6\alpha_{\rm R})}{(p+4)(p+5)} \\ \tilde{\xi}_{\rm RM} &= \frac{2p+13+2\alpha_{\rm R}}{p+4} - \frac{6(2p+13+\alpha_{\rm R}p+6\alpha_{\rm R})}{(p+4)(p+5)} \end{aligned} \quad (13)$$

where $\alpha_{\rm R}$ is the radio spectral index and p is assumed to be the same for radio and X-ray emitting electrons[7], and we have used a tilde to distinguish the synchrotron X-ray model.

5.4 Comparison with observations

In the previous sections we have shown how different theoretical models for the emission processes responsible for the observed radio and X-ray emission from black holes can be directly translated into predictions for the observable correlation coefficients $\xi_{\rm RX}$ and $\xi_{\rm RM}$ (see eq. 3). The relatively tight observational constraints on these indices that we have derived in section 3 can therefore be used to directly test these models. The theoretical coefficients for different models are shown in Figure 5. The circles and the squares denote inefficient and efficient disc accretion respectively. Diamonds represent synchrotron X-rays from the jet. Open and closed symbols are for flat ($\alpha_{\rm R} = 0$) and steep ($\alpha_{\rm R} = 0.5$) spectrum sources, respectively. All model coefficients are calculated assuming $p = 2$ (but see §6.4 for a discussion of steeper electron distributions as due, for example, to the effects of cooling). To highlight the sensitivity of the coefficients to variations in $\alpha_{\rm R}$, we also plotted the tracks in $\xi_{\rm RX} - \xi_{\rm RM}$ space for changes in $\alpha_{\rm R}$ between 0 and 0.5.

For the models in which X-rays are produced by radiatively inefficient accretion, we have $q = 2.3$ and $\partial \ln \phi_B / \partial \ln \dot{m} = -\partial \ln \phi_B / \partial \ln M = 0.5$ (see §5.2.2). The predicted coefficients for both flat and steep spectrum sources lie roughly within the 3σ contours of the observed sample. Thus, radiatively inefficient accretion is consistent with the observations. This conclusion is also true for the general class of models for which $q = 2$.

For the standard disc–corona model, we have $q = 1$ (high radiative efficiency) and $\partial \ln \phi_B / \partial \ln \dot{m} = -\partial \ln \phi_B / \partial \ln M = 0.5$ (see §5.2.1). The model predictions fall well outside the 3σ contours of the data and are therefore inconsistent with the observations.

For the models in which the X-rays are produced by optically thin synchrotron emission from the jet itself, the flat spectrum model predictions are marginally consistent with the data (the model point is close to the 3σ contour), while the steep spectrum model point lies well outside the 3σ contour.

These results suggest that, in a statistical sense, the correlations between radio luminosity, X-ray luminosity and mass of active black holes require a radiatively inefficient accretion flow coupled with a (scale invariant) synchrotron emitting jet. It is important to stress here that this result does not suggest that the ADAF model for the accretion flow is the correct one, and convection and/or powerful outflows are unimportant. In fact, the nature of the radio emission and the mere existence of the fundamental plane are clear indications that the full dynamical model for the accretion flow should at some level include, in a self-consistent manner, the effects of the backreaction from the outflowing gas. However, our results rather dictates that the radiative efficiency of the flow *must* be low. This conclusion holds over the observed range of $L_{\rm X}/L_{\rm Edd}$, and therefore for sources which are substantially sub-Eddington. In §6.6 we discuss what should be expected from similar studies performed on samples that include a larger number of very luminous black holes.

The jet synchrotron model for the X-ray emission with $p = 2$ is only marginally consistent with the data. However, steeper electron distributions ($p = 3$, for example) do predict values for the correlation coefficient that are well within our 3-σ contours. An assessment of the relevance of such models should be made taking in due account the effect of cooling, as we discuss in §6.4.

6 DISCUSSION

The main result of our work is the discovery of a "fundamental plane" of black hole activity. That is, if we define the instantaneous state of activity of a black hole of mass M (in units of solar masses), by the radio luminosity at a fixed frequency (for example at 5 GHz), and by the hard X-ray luminosity (for example in the 2-10 keV energy band) of its compact core, and represent such an object as a point in the three-dimensional space ($\log L_{\rm R}, \log L_{\rm X}, \log M$), all the points representing black holes (either of stellar mass or supermassive) will lie preferentially on a plane, described by equation (5).

We note that in the case the radiatively inefficient disc model ($q = 2.3$) the fundamental plane equation (5) implies that the radio luminosity satisfies:

$$L_{{\rm R},q=2.3} \propto \dot{m}^{1.38} M^{1.38} = \dot{M}^{1.38}, \quad (14)$$

i.e., $L_{\rm R}$ scales with the *physical accretion rate* only. This is very

[7] This implies that radiative cooling must either be negligible for the region of the jet where the X-rays are produced, leaving $p \sim 2$ over the entire spectrum, or that cooling and continuous injection have produced a universal power-law with a slope of order $p \sim 3$. This limitation, while severe, cannot be avoided because particle transport including the effects of radiative cooling cannot be formulated in a simple scale invariant fashion.

close to the predicted dependence of $L_{\rm R} \propto \dot{M}^{1.42}$ from 5.1 for the canonical parameter choice of $\alpha = 0$, $p = 2$, and $\phi_B \propto M^{-1/2}\dot{m}^{1/2}$, for which the kinetic jet power $W_{\rm jet}$ is directly proportional to the physical accretion rate, $W_{\rm jet} \propto \dot{M}$ (see also Falcke & Biermann 1995). Then, the total power released by the accretion/jet system may be written as $W_{\rm tot} \simeq \dot{M}c^2 = L_{\rm bol} + W_{\rm jet} + W_{\rm adv,conv}$, where the first term on the right hand side is the total radiated luminosity and the last one include contributions from the energy advected and/or stored in the convective motions. Our results suggest that the flow must be radiatively inefficient, therefore, for small enough accretion rates we have $L_{\rm bol} \simeq \dot{M}\dot{m}c^2 \ll \dot{M}c^2 \sim W_{\rm jet} + W_{\rm adv,conv}$. On the other hand, $W_{\rm jet} \propto W_{\rm adv,conv} \propto \dot{M}c^2$. Therefore, the issue of what the relative fraction of the total accretion energy dissipated into the jet is (or, alternatively, of when a source is "jet dominated"; Fender, Gallo & Jonker 2003; Falcke, Körding & Markoff 2003) reduces to the determination of the value of the constant $W_{\rm jet}/W_{\rm adv,conv}$. This requires the knowledge of the structure functions ψ in eq. (6), i.e. the specification of a jet model or the direct measure of the total kinetic power carried by the jet, together with a dynamical model for the disc-jet coupling, which is clearly beyond the scope of this paper.

6.1 The thickness of the fundamental plane

The fundamental plane defined in eq. (5) is not, however, razor thin. The sources are substantially scattered around it, with a dispersion $\sigma = 0.88$ in $\log L_{\rm R}$ (corresponding to a dispersion of $\sigma_\perp = 0.62$ perpendicular to the plane). Such a scatter is not at all surprising. Theoretically, it can be explained in large part by the scatter in the radio spectral index $\alpha_{\rm R}$. For example, if we consider the ADAF ($q = 2.3$) model with fixed $p = 2$, we expect the theoretical relationship $L_{\rm R} = (0.62{+}0.29\alpha_{\rm R})\log L_{\rm X}{+}(0.80{-}0.62\alpha_{\rm R})\log M{+}b_{\rm R}$. For the sake of simplicity, let us assume now that the unknown radio spectral index of all the observed sources is normally distributed, with $\alpha_{\rm R} = \langle\alpha_{\rm R}\rangle \pm \sigma_\alpha$. In order to fit the observed data, we need $\langle\alpha_{\rm R}\rangle \approx 0$ and $b_{\rm R} \approx 7$. The dispersion in the radio luminosity due to the dispersion in the unknown parameter $\alpha_{\rm R}$ is then $\sigma_{\rm R} \gtrsim \sigma_\alpha\sqrt{0.33^2\,(\Delta\log M)^2 + 0.29^2\,(\Delta\log L_{\rm X}/M)^2} \sim 2\sigma_\alpha$ where $2\Delta\log M$ is the range in M and $2\Delta\log L_{\rm X}/M$ the range in luminosity spanned by our sample. Thus, a dispersion in the unknown radio spectral index of ≈ 0.3 (consistent with the observations), can give a large contribution to the observed intrinsic scatter.

In addition to the scatter produced by the diversity in $\alpha_{\rm R}$ (which introduces scatter in the fundamental plane relation simply by the fact the *orientation* of the plane is slightly different for different $\alpha_{\rm R}$) the *intercept* $b_{\rm R}$ of the plane also varies as we look at different jet models and different spectral indices. It is not clear a-priori how much it does so, as this depends on how the shape functions ψ_f (see section 5.1) vary in order to produce the different $\alpha_{\rm R}$. While for one spectral class with uniform $\alpha_{\rm R}$ the normalization cancels out when determining the correlation coefficients, this is not true when comparing jets from different spectral classes, i.e., with varying $\alpha_{\rm R}$. The fact that the scatter in the relation is moderate indicates, however, that the change in ψ_f over the range of radio spectral slopes that enter our sample is also moderate.

Ideally, we should therefore restrict the above analysis to subclasses of sources which follow a very narrow range in $\alpha_{\rm R}$. However, at the current stage the data do not allow such a division, both because the sample is too small and because the spectral indices are often not known to an accuracy that would allow such a treatment. The rough division of our sample into flat and steep spectrum sources nonetheless shows that such a treatment is possible and does lead to a reduction in scatter in the well defined and well sampled class of flat spectrum sources, for which we can be confident that the radio emission does indeed originate in the self-absorbed core of the jet (a prerequisite of the scale invariance model by Heinz & Sunyaev, 2003).

A major source of scatter could be relativistic beaming, that we discuss in the following section. Also to be taken into account is the influence of the black hole spin on jet formation (Blandford & Znajek 1977; Koide et al. 2002). While we still expect the accretion disc to have significant influence on the jet power, as the magnetic field necessary to tap the black hole rotational energy must be provided and/or confined by the accretion disc (thus setting the field strength and the jet power; see Livio, Ogilvie & Pringle 1999; Meier 2001), the spin itself will enter as a sensitive parameter into the radio luminosity as well, introducing scatter in any correlation. Once again, strong future constraints on the tightness of this relation may help constrain the possible influence of black hole spin (see e.g. Fender 2003, for a discussion of the GBH case).

6.2 Relativistic beaming and selection effects

Because the jets that dominate radio emission from active black holes are known to be relativistic, Doppler boosting of synchrotron radiation (relativistic beaming) must be taken into account when studying these sources.

For the purpose of our study it is of primary importance to avoid strongly beamed sources, whose intrinsic (unbeamed) radio luminosity can be difficult to infer. This is the reason why BL Lac object have been excluded from our study. Furthermore, it is also important to take into account possible strong selection effects due to relativistic beaming, that would skew the observed correlations. Then, in a sample of randomly oriented jetted sources (but without the aligned ones), relativistic beaming should be an additional source of scatter in any correlation involving radio luminosities, the magnitude of which depends on the average relativistic speed of the jets.

For the SMBH in our sample, the first selection criterion is the availability of a mass measurement of the central black hole. Thus, the main selection biases do not come from flux limits, and no preferential selection of bright (beamed) sources should be operating, although anti-selection effect might be present.

Possible contaminations from beamed sources, however, could still be present among flat spectrum nearby LLAGN or type 1 Seyfert (we have 27 of them in the sample), given the current uncertainties on the exact nature of their radio emission. Nevertheless, there are many reasons to believe that these sources are not biased towards jet axes close to the line of sight. Flat spectrum LLAGN were originally selected in the optical band, from the Palomar spectroscopic survey (Ho, Filippenko, & Sargent 1997a). Many of those type 1 low-luminosity Seyfert and LINERS do indeed possess double-peaked broad emission lines (Ho et al. 2000), clearly indicating a non negligible inclination angle. The radio properties of a number of these sources were also studied by Nagar et al. (2002). They found that LLAGN lie on the extrapolation of the FR I/FR II correlations in the $L_{\rm R} - L_{H\alpha}$ plane, while a substantial offset would be expected if they were all strongly affected by beaming. Once again, we are led to the conclusion that nearby LLAGN and Seyfert 1 included in our sample have a random orientation angle, that should disfavor strongly beamed sources. Finally we note that even if a few of these source were indeed strongly Doppler boosted, their small number will not affect significantly the measured value of a correlation coefficient calculated in logarithmic space (logarithmic weighting).

Selection effects due to beaming in Galactic sources may be more subtle. Due to the overall scaling of radio luminosity with mass, GBH are expected to be on average more radio quiet than SMBH (see also §6.6). It is indeed well known that galactic X-ray binaries are difficult to detect in the radio band, and this might already determine a selection bias towards beamed sources. In particular, sources selected from GBI monitoring (see §2.2) might be more beamed. If indeed GBH were all affected by strong selection biases toward beamed emission, the derived correlation coefficients of the fundamental plane, $\xi_{\rm RM}$ in particular, might be incorrect. However, we know from observation of proper motion during radio outbursts that the jets of the classical microquasars GRO J1655-40 and GRS 1915+105 have large angle with the line of sight (see e.g. Fender 2003). Furthermore, for all the other GBH in our sample, apart from LS5039, orbital parameters have been inferred from optical spectroscopy, and in none of them the inferred inclination angle appears to be small. Therefore, unless the black hole jets are all misaligned with the orbital angular momentum (Maccarone 2002), we can exclude that strong beaming affects our sample.

A similar conclusion had already been reached by an accurate study of the observed scatter (~ 0.7) about the $L_{\rm R}-L_{\rm X}$ correlation in a larger sample of low/hard state GBH (Gallo, Fender, & Pooley 2003). An analogous argument could be put forward for our entire sample, with the similar conclusion (given the similar amount of scatter found here) that the maximum Doppler factor should not be too large. This conclusion would be further strengthen by noting that the observed scatter about the fundamental plane is not much larger than what expected from the intrinsic scatter in the radio spectral index $\alpha_{\rm R}$ (see §6.1). However, precise constraints on the Doppler factor could only be obtained by analyzing more carefully selected samples with well determined (possibly fixed) radio spectral indices.

6.3 Steep spectrum sources

For the steep spectrum sources in our sample, the origin of the radio emission is not entirely clear. Steep spectra in general imply optically thin emission. This could be an indication that the emission is dominated by regions far away from the central engine, e.g. in the diffuse extended radio lobes or hot spots. This would prohibit any treatment that makes use of the scale invariant model, though scaling arguments for the large scale emission still apply (Heinz 2002). Steep spectrum sources should then be excluded from the sample completely, and the fact that they still fit into the plane would then mostly be due to selection effects. It should be noted that in this case the radio luminosity should strongly correlate with the black hole mass (which determines the kinetic jet power $W_{\rm jet}$ and thus the large scale radio luminosity), while it should not be related to the instantaneous X-ray flux, because the radio lobes reflect the mean power output by the central source, averaging out its temporal variability. We expect this to be a problem for Galactic black hole sources, where we have lower resolving power. For supermassive black holes and for nearby LLAGN in particular, we can be more confident that the large scale emission is well resolved and thus does not contribute to the core emission used in our sample.

It is also possible that some of the steep spectrum sources can be associated to core jet emission which is optically thin at radio frequencies, i.e., their self-absorption break lies below 5 GHz. Because we would expect the self-absorption break frequency to be lower for higher M and lower accretion rates $\dot{m}$ (Heinz & Sunyaev 2003), this effect would imply that steep spectra should predominantly be observed in SMBH which are relatively X-ray dim. While the trend with $L_{\rm X}$ is not clear in the data, the fact that the steep spectrum sources in our sample almost exclusively belong to the SMBH class does suggest that at least some of the sources in the sample might indeed be core dominated steep spectrum sources, for which the theoretical analysis of §5 holds.

6.4 X-ray emission from jets

Our analysis, taken at face value, does suggest that accretion models for the origin of the X-ray emission fit the data somewhat better than pure jet models. However, at X-ray energies the effects of cooling on the particle spectrum cannot be ignored. In the context of scale invariant models, taking cooling into account is not possible. Proper treatment of particle transport including the effects of cooling may lead to different results for the synchrotron X-ray model. In fact, simply using $p = 3$ in eq. (13) (as expected in a continuous particle injection model with cooling) moves the flat spectrum point close to the 1σ contour of the observed correlation in Fig. 5.

For the case of the galactic black hole GX 339-4 in the hard state, where the radio–X-rays correlation is well established, Markoff et al. (2003) were able to fit the observed slope ($\xi_{\rm RX,\,339} \simeq 0.71$) with a synchrotron X-ray model assuming $p = 2.15$ (and thus $\alpha_{\rm X} = 0.58$, which is also close to the average slope of the X-ray spectral index of the source in the hard state). Here we have found that, in a statistical sense, higher values of p are needed to explain the observed correlation for the entire sample in the framework of the jet synchrotron model for the X-ray emission.

Furthermore, for $p = 2$ the X-ray synchrotron luminosity from the jet scales like $L_{\rm X,synch} \propto M^{1.25}$, while the disc X-ray luminosity follows $L_{\rm X,disc} \propto M$. Thus, *if* the X-ray emission in GBH jets like GX 339-4 were indeed due to synchrotron emission, we would expect an even stronger contribution from synchrotron X-rays relative to the disc emission in AGNs with the same accretion rate, where the general wisdom (mainly based on accurate analysis of detailed X-ray spectra) is still that the X-rays originate predominantly in the disc. For $p = 3$, on the other hand, the synchrotron X-rays follow $L_{\rm X,synch} \propto M$, and the relative contribution from jet and disc will be independent of M.

Finally, the X-ray spectral variability behaviour of both GBH and Seyfert galaxies is consistent with pivoting of the spectrum at X-ray energies. If the X-ray emission is produced by synchrotron radiation and there is no cooling break at longer wavelengths, such a power-law variability would imply a radio variability which is orders of magnitude larger than observed (see discussion in Zdziarski et al. 2003).

It seems, therefore, that *if* the X-ray emission in some of the sources is dominated by synchrotron emission from the jet, the effects of cooling must play an important role in determining the observed correlation. In the context of the scale-invariant model, it is rather problematic to take cooling into account; this is why a theoretical assessment of the role of the cooling on the observed correlation is beyond the scope of this paper.

6.5 Estimating black holes masses and the nature of ULXs

Due to the intrinsic scatter, the predictive power of the $\log M - \log L_{\rm X} - \log L_{\rm R}$ relation is currently limited in scope. Nonetheless, from the fundamental plane equation (5), we can derive a formal relationship between the observed fluxes in the radio (at 5 GHz) and in the X-ray (2-10 keV) band (in erg s^{-1} cm^{-2}), the distance to a source D (in Mpc) and its unknown mass. We obtain

$$\log M \simeq 16.3 + \log D + 1.28(\log F_{\rm R} - 0.60 \log F_{\rm X}) \pm 1.06. \quad (15)$$

In particular, we can predict in which region of $\log L_{\rm R} - \log L_{\rm X}$ space we would expect to find intermediate mass black holes, if they exist, and specifically, where we would expect Ultra-Luminous X-ray sources (ULX; Makishima et al. 2000) based on their X-ray flux, should they be intermediate mass black holes, as opposed to intrinsically beamed low mass black holes.

A clear prediction of the fundamental plane equation in this sense is that, if ULX are stellar mass objects (with $M < 30$), and their radio emission is not strongly Doppler boosted, there is an upper limit to their radio flux at 5 GHz. For example, a ULX with and X-ray luminosity (in the 2-10 keV band) of 10^{40} ergs s^{-1} at a distance of 10 Mpc will have

$$\log(F_{\rm R}/{\rm Jy}) \lesssim -6.5 - 2\log(D/10) + 0.6(\log L_{\rm X}/40) \pm 0.9 \quad (16)$$

so its flux will be at most few microJansky.

As an example, we refer to the recent claim of the observation of synchrotron radio emission from the ULX 2E 1400.2-4108, in the dwarf irregular galaxy NGC 5408 (at a distance of ~ 4.8 Mpc) (Kaaret et al. 2003). The observed radio (0.26 mJy at 4.8 GHz) and X-ray fluxes (2.7×10^{-12} erg s^{-1} cm^{-2} in the 0.3-8 keV band), if indeed both associated with a compact source at the distance of NGC 5408, would imply a mass of $\log M \simeq 4 \pm 1$. However, we should stress here that such an estimate only holds *if the radio emission is not beamed*. The uncomfortably high value for the estimated mass, the steep inferred radio spectral index and the radio to X-ray flux ratio, all suggest that the observed intensity of the radio emission in this source may be Doppler boosted by a relativistic jet pointing in our direction as already suggested by Kaaret et al. (2003).

6.6 Accretion mode changes

It is well accepted, both from theory and observations, that accretion can proceed in different modes (or states), with different radiative efficiencies and spectral properties (Abramowicz 1998; Done 2002; Frank, King, & Raine 2002; Narayan 2002), mainly driven by variations of the dimensionless accretion rate $\dot{m}$. Here we have demonstrated (§5) that the correlation between radio and X-ray luminosity in GBHs and SMBHs can provide valuable constraints on the emission mechanisms in these bands and on the physics of accretion. We have shown how low radiative efficiency accretion models can possibly provide the underlying scalings that most easily explain the properties of the observed fundamental plane. Radiatively efficient thin disc–corona systems are clearly inconsistent with the data. The only possibility for these models to be reconciled with our observations would entail a highly radiatively inefficient corona, where most of the dissipated magnetic energy is converted into bulk kinetic energy of outflowing gas (Beloborodov 1999), as described by Merloni & Fabian (2002). This would require some specific model for the magnetic dissipation processes, and for their scaling with M and $\dot{m}$, which are currently unknown.

However, because both such modes of accretion are expected to occur only below accretion rates $\lesssim$ few percent of Eddington, we would expect the $\log M - \log L_{\rm R} - \log L_{\rm X}$ correlation to break down at around this limit. In other words, we should expect the QSOs and the bright Seyferts in our sample, which occupy the region of high accretion rates and are independently known to have spectral characteristics inconsistent with models of low radiative efficiency, to depart from the observed correlations. Also in GBHs, it has indeed been shown that the correlation between radio and X-ray luminosity breaks down as the sources switch to their high states (Maccarone 2003; Gallo, Fender, & Pooley 2003). In particular, high luminosity states of GBH (high or very high states) show highly variable radio fluxes and radio to X-ray ratios (Mirabel & Rodriguez 1994; Fender et al. 1999). If this reflects a general property of the disc–jet coupling at high accretion rates, a substantial increase in the scatter should appear above the critical accretion rate.

In order to illustrate this point further, in Figure 7 we plot, as a function of the ratio $L_{\rm X}/L_{\rm Edd}$, the radio luminosity divided by $M^{1.38}$ (such a scaling for the radio luminosity with mass is obtained directly from the fundamental plane equation (5) by imposing that the X-ray luminosity scales linearly with black hole mass). As indeed expected, by rescaling the radio luminosity in such a way all the different tracks corresponding to different mass bins in Fig. 3b collapse into a single one (with some residual scatter). The region between the two vertical lines corresponds to the expected values of $L_{\rm X}/L_{\rm Edd}$ above which a change of accretion mode, from radiatively inefficient to standard radiatively efficient is expected to occur. Our SMBH sample is still limited in order to test whether such a change is observed. In fact, we select out of our sample the majority of bright quasars, both radio quiet and radio loud, because of the lack of a reliable mass estimates for these sources. However, there is indeed a hint of an apparent increase in the scatter about the correlation, above the critical accretion rates, as seen in Figure 7.

We may thus speculate that the famous (and still much debated, see e.g. Cirasuolo et al. 2003) radio loud/radio quiet dichotomy of quasars will appear only at the highest values of $\dot{m}$, and be caused mainly by a switch of accretion mode analogous to the high/very high transition in GBH. At low accretion rates, black holes seem to follow the more regular behavior circumscribed by the fundamental plane of eq. (5). Such sources not only tend to be radio loud (Ho & Peng 2001; Ho 2002a), but also their radio loudness parameter, $R_{\rm X}$ (here defined as the ratio of radio to X-ray luminosity), obeys the following scaling: $R_{\rm X} \equiv L_{\rm R}/L_{\rm X} \propto L_{\rm X}^{-2/5} M^{4/5}$. Therefore, the smallest the X-ray luminosity, the more radio loud these sources are (Ho 2002a). In this regime, no dichotomy has to be expected, as already suggested by Nagar et al. (2002).

7 SUMMARY

We have shown how the coupling between accretion flows and jet emission in black holes can be understood by studying large samples of *both* galactic (GBH) and supermassive (SMBH) black holes with measured mass, observed at both radio and X-ray wavelengths.

We have compiled, from the existing literature, a sample of ∼100 supermassive black holes and ∼50 different observations of galactic, stellar mass black holes. We required that the SMBH have a reliable measure of the central black hole mass, either (preferentially) direct, via high resolution kinematics studies of surrounding stars and gas or reverberation mapping of the broad line region (for luminous Seyfert 1 galaxies and Quasars), or, indirectly, thanks to the empirical correlation between black hole masses and central velocity dispersion. Although such selection criteria introduce a num-

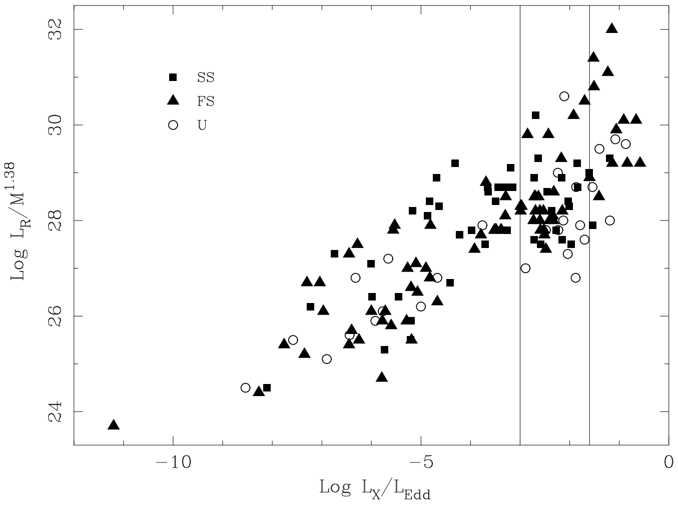

Figure 7. The radio luminosity $\log L_{\rm R}$, divided by $M^{1.38}$ as a function of the ratio $L_{\rm X}/L_{\rm Edd}$. Solid squares are for steep spectrum sources, solid triangles for flat spectrum ones and open circles for sources with undetermined radio spectral index. Two vertical lines mark the boundary of the region where we expect the critical luminosity for the mode change between radiatively inefficient and efficient accretion. The scaling for the radio luminosity with mass is obtained directly from the fundamental plane equation (5) by imposing that the X-ray luminosity scales linearly with black hole mass.

ber of biases in the final distribution of M, which are difficult to control, our final sample spans a large enough range in both mass and accretion rate to unveil major trends in the physical properties of active black holes. This is a crucial point, and represents the main novelty of our approach. Most previous studies on the subject have only considered correlations of jet (radio) luminosity with black hole mass or with luminosity in other wavewbands (and hence with accretion rate) separately.

We have performed a partial correlation analysis on the sample, and concluded that the radio luminosity is strongly correlated with *both* black hole mass *and* X-ray luminosity, while in turn, the X-ray luminosity correlates with both mass and radio luminosity. In light of this, we have carried out a multivariate linear regression analysis and derived the best fit correlation coefficient between radio luminosity, X-ray luminosity and black hole mass.

The data from the entire sample allow us to put tight constraints on the correlation coefficients. Remarkably, we find that the sources lie preferentially on a plane ("the fundamental plane of black hole activity") in the three dimensional $(\log L_{\rm R}, \log L_{\rm X}, \log M)$ space, described by the equation $\log L_{\rm R} = (0.60^{+0.11}_{-0.11}) \log L_{\rm X} + (0.78^{+0.11}_{-0.09}) \log M + 7.33^{+4.05}_{-4.07}$. The scatter around this plane is, however, significant ($\sigma_{\rm R} = 0.88$).

From a theoretical point of view, these results clearly suggest that the *ansatz* of scale invariance for the disc–jet coupling (Heinz & Sunyaev 2003) captures the main physical properties of such systems. Thus, a universal theoretical scaling between the radio flux at a given frequency and both mass and accretion rate can be derived, *independently of the jet model*, with scaling indices that depend only on the (observable) spectral slope of the synchrotron emission in the radio band, and on the accretion mode. Also, it is possible to predict the correct amount of scatter for any such relationship.

By comparing the observationally derived correlation coefficients to the theoretically predicted ones, we are able to put constraints on accretion models and on the disc–jet coupling. We demonstrate that the X-ray emission from black holes accreting at less than a few per cent of the Eddington rate cannot be produced by radiatively efficient accretion, while radiatively inefficient accretion flows agree well with the data. The optically thin X-ray jet synchrotron emission model is only marginally consistent with the observed correlation; however, cooling of the electrons should be properly taken into account before drawing a firmer conclusion on the issue.

The fundamental plane equation also implies that low luminosity black holes should be more and more radio loud as the accretion rate decreases, as observed (Ho 2002a). The possible dichotomy between radio quiet and radio loud Quasars could instead be due to a switch of accretion mode at the highest accretion rates. Therefore, more accurately selected samples of more luminous sources, including a significant number of both radio quiet and loud quasars with well determined radio spectral properties, should allow the observation of bends, discontinuities or even bifurcations of the fundamental plane associated with accretion mode switches and with the turning on and off of the most powerful radio sources.

NOTE ADDED IN PROOFS

After the submission of this manuscript another work has appeared as preprint (Falcke, Körding, & Markoff 2003), that is similar in scope, and reaches very similar conclusions about the scale invariant properties of low luminosity black holes.

ACKNOWLEDGMENTS

We are grateful to Marat Gilfanov for his useful comments. We thank Eric Feigelson and the Statistical Consulting Center for Astronomy (SDASS) for providing the code for the partial correlation analysis and some advice on its usage. This research has made use of the NASA/IPAC extragalactic database (NED), which is operated by the Jet Propulsion Laboratory, Caltech, under contract with NASA. We have also made use of LEDA, supplied by the LEDA team at the CRAL-Observaoire de Lyon. This research has made use of the publicly available radio monitoring data from the Green Bank Interferometer. The Green Bank Interferometer is a facility of the National Science Foundation operated by the NRAO in support of NASA High Energy Astrophysics programs. This research made use of results provided by the ASM/RXTE teams at MIT and at the RXTE SOF and GOF at NASA's GSFC.

REFERENCES

Abramowicz M. A., Chen X., Kato S., Lasota J.-P., & Regev O., 1995, ApJL, 438, L37.

M.A. Abramowicz, 1998, in *Theory of Black hole accretion disks*, eds. M.A. Abramowicz, G. Bjornsson, and J.E. Pringle. (CUP, 1998)

Akritas, M. G. & Siebert, J., 1996, MNRAS, 278, 919

Allen S. W., Fabian A. C., Johnstone R. M., Arnaud K. A. & Nulsen P. E. J., 2001, MNRAS, 322, 589

Baganoff et al., 2001, Nature, 413, 45.

Balbus S. A. & Hawley J. F., 2002, ApJ, 573, 749

Barth, A. J., Ho, L. C., & SArgent, W. L. W., 2002, AJ, 124, 2607

Bassani, L., Dadina, M., Maiolino, R., Salvati, M., Risaliti, G., della Ceca, R., Matt, G., & Zamorani, G., 1999, ApJS, 121, 473

Becker, R. H., White, R. L., & Edwards, A. L., 1991, ApJS, 75, 1

Beckert T. & Duschl W. J., 2002, A&A, 387, 422

Begelman M. C., Blandford R. D., & Rees M. J., 1984, Rev. Mod. Phys., 56, 255
Beloborodov A. M., 1999, ApJ, 510, L123
Blandford R. D. & Königl A., 1979, ApJ, 232, 34
Blandford R. D. & Znajek R. L., 1977, MNRAS, 179, 433
Brinkmann W., Laurent-Muehleisen S. A., Voges W., Siebert J., Becker R. H., Brotherton M. S., White R. L., & Gregg M. D., 2000, A&A, 356, 445
Churazov E., Forman W., Jones C. & Böhringer H., 2003, ApJ, 590, 225
Corbel, S., Nowak, M. A., Fender, R. P., Tzioumis, A. K., & Markoff, S., 2003, A&A, 400, 1007
De Rosa, A., Fabian, A. C., & Piro, L., 2002, MNRAS, 334, L21
De Zeeuw T., 2003, to appear in Carnegie Observatories Astrophysics Series, Vol. 1: "Coevolution of black holes and galaxies" ed. L.C. Ho (Cambridge: CUP)
Dhawan, V., Pooley, G. G., Ogley, R. N., & Mirabel, I. F., 2000, IAUC 7395
Di Matteo, T., Allen, S. W., Fabian, A. C., Wilson, A. S., & Young, A. J., 2003, ApJ, 582, 133
Di Matteo, T., Celotti, A., & Fabian, A. C., 1999, MNRAS, 304, 809
Di Matteo T., Fabian A. C., Rees M. J., Carilli C. L., & Ivison R. J., 1999, MNRAS, 305, 492
Di Matteo, T., Johnston, R. M., Allen, S. W., & Fabian, A. C., 2001, ApJL, 550, L19
Dolan J. F., 1992, ApJ, 384, 249.
Done, C., 2002, Phil. Trans. of the Royal Society, A360, 1967.
Fabbiano, G., Kim, D.-W., & Trincheri, G., 1992, ApJS, 80, 531
Fabbiano, G., et al., 2003, ApJ, 588, 175
Falcke, H. & Biermann, P. L., 1995, A&A, 293, 665
Falcke, H. & Biermann, P. L., 1996, A&A, 308, 321
Falcke H., Körding E. & Markoff S., 2003, A&A, submitted, astro-ph/0305335
Falcke, H., Malkan, M. A., & Biermann, P. L., 1995, A&A, 298, 375
Falcke, H., Nagar, N. M., Wilson, A. S., & Ulvestad, J. S., 2000, ApJ, 542, 197
Fasano G. & Vio R., 1988, Newsletter of the Working Group for Modern Astronomical Methodology, 7, 2
Fender R. P., 2003, to appear in 'Compact Stellar X-Ray Sources', eds. W.H.G. Lewin and M. van der Klis, Cambridge University Press. astro-ph/0303339
Fender R. P., Gallo E., Jonker P. G., 2003, MNRAS, in press. astro-ph/0306614
Fender R. P., Garrington S. T., McKay D. J., Muxlow T. W. B., Pooley G. G., Spencer R. E., Stirling A. M., & Waltman E. B., 1999, MNRAS, 304, 865
Fender R. P., 2001, MNRAS, 322, 31
Fender, R. P., Hjellming, R. M., Tilanus, R. P. J., Pooley, G. G., Deane, J. R., Ogley, R. N., & Spencer, R. E., 2001, MNRAS, 322, L23
Fender, R. P. & Kuulkers, E., 2001, MNRAS, 324, 923
Ferrarese L., 2002, in "Current High Energy Emission around Black Holes", ed. C.-H. Lee (Singapore: World Scientific) in press. astro-ph/0203047
Ferrarese, L. & Merritt, D., 2000, ApJL, 539, L9
Filippenko A. V. & Chornock R., 2001, IAUC 7644
Franceschini, A., Vercellone, S., & Fabian, A. C., 1998, MNRAS, 297, 817
Frank, J., King, A., & Raine, D., 2002, *Accretion power in astrophysics*, 3rd ed. (CUP, 2002)
Frontera et al., 2001, ApJ, 561, 1006
Gallo, E., Fender, R. P., & Pooley, G. G., 2002, in 'Proceedings of the 4th Microquasar Workshop', Eds. P.Durouchoux, Y.Fuchs and J.Rodriguez. Center for Space Physics: Kolkata (India), p.201.
Gallo, E., Fender, R. P., & Pooley, G. G., 2003, MNRAS, in press. astro-ph/0305231
Gebhardt, K. et al. ApJL, 539, L13
George, I. M., Turner, T. J., Yaqoob, T., Netzer, H., Laor, A., Mushotzky, R. F., Nandra, K., & Takahashi, T., 2000, ApJ, 531, 52
Giovannini, G., Cotton, W. D., Feretti, L., Lara, L., & Venturi, T., 1998, ApJ, 493, 632
Gondoin, P., Orr, A., Lumb, D., & Santos-Leo, M., 2002, A&A, 388, 74
Gregory, P. C. & Condon, J. J., 1991, ApJS, 75, 1011
Greiner, J., Cuby, J. G., & McCaughrean, M. J., 2001, Nature, 414, 522
Griffith, et al., 1995, ApJS, 97, 347
Grimm, H.-J., Gilfanov, M., & Sunyaev, R., 2002, A&A, 391, 923
Haardt, F. & Maraschi, L., 1991, ApJL, 380, L51
Hanson M. M., Still M. D., & Fender R. P., ApJ, 541, 308
Hawley J. F. & Balbus S. A., 2002, ApJ, 573, 749
Heinz, S., 2002, A&A, 388, 40
Heinz, S. & Sunyaev, R. A., MNRAS, accepted. astro-ph/0305252
Héraudeau, Ph. & Simien, F., 1998, A&ASS, 113, 317
Ho, L. C., 2002a, ApJ, 564, 120
Ho, L. C., Filippenko, A. V., & Sargent, W. L., 1997b, ApJ, 487, 568
Ho, L. C., Filippenko, A. V., & Sargent, W. L., 1997a, ApJS, 112, 315
Ho, L. C. & Peng, C. Y., 2001, ApJ, 555, 650
Ho L. C., Rudnick G., Rix H.-W., Shields J. C., McIntosh D. H., Filippenko A. V., Sargent W. L. W. & Eracleous, M., ApJ, 541, 120
Ho, L. C., Terashima, Y., & Ulvestad, J. S., 2003, ApJ, 589, 783
Ho, L. C. & Ulvestad, J. S., 2001, ApJS, 133, 77
Ho, L. C., et al., 2001, ApJL, 549, L51
Igumenschev I. V. & Abramowicz M. A., 2000, ApJS, 130, 463
Isobe, T., Feigelson, E. D., & Nelson, P. I., 1986, ApJ, 306, 490
Kaaret P., Corbel S., Prestwich A. H., & Zezas A., 2003, Science, 299, 365
Kaspi, S., Smith, P. S., Netzer, H., Maoz, D., Jannuzi, B. T., & Giveon, U., 2000, ApJ, 533, 631
Kellermann K. I., Sramek R., Schmidt M., Shaffer D. B., & Green R., 1989, AJ, 98, 1195
Koide S., Shibata K., Kudoh T. & Meier D. L., 2002, Science, 295, 1688
Kojoian, G., Tovmasian, Kh. M., Dickinson, D. F., & Dinger, A. S. C., 1980, AJ, 85, 1462
Kormendy, J. & Richstone, D., ARA&A, 33, 581
Lacy, M., Laurent-Muehleisen, S. A., Ridgway, S. E., Becker, R. H., & White, R., 2001, ApJL, 551, L17
Laor, A., 2000, ApJL, 543, L111
Lawson, A. J., & Turner, M. J. L., MNRAS, 288, 920
Leighly, K. M., 1999, ApJS, 125, 317
Livio M., Ogilvie G. I. & Pringle J. E., 1999, ApJ, 512, 100
Loewenstein, M., Mushotzky, R. F., Angelini, L., Arnaud, K. A., & Quataert, E., 2001, ApJL, 555, L21
Maccarone T., 2002, MNRAS, 336, 1371.
Maccarone T., 2003, MNRAS, submitted.
Magorrian, J. et al., 1998, AJ, 115, 2285
Makishima K. et al., 2000, ApJ, 535, 632
Markoff S., Falcke H., & Fender R., 2001, A&A, 372, L25
Markoff, S., Nowak, M., Corbel, S., Fender, R., & Falcke, H., 2003, A&A, 397, 645
McLure, R. J. & Dunlop, J. S., 2001, MNRAS, 327, 199
Meier D. L., 2001, ApJL, 548, L9
Melia, F. & Falcke, H., 2001, Ann. Rev. Astron. Astrophys., 39, 309
Merloni, A., 2003, MNRAS, 341, 1051
Merloni, A. & Fabian, A. C., 2002, MNRAS, 332, 165
Merritt, D. & Ferrarese, L., 2001, MNRAS, 320, L30
Miley G. K., 1980, ARA&A, 18, 165
Mirabel, I. F. & Rodriguez, L. F., 1994, Nature, 371, 46
Moran, E. C., Kay, L. E., Davis, M., Filippenko, A. V., & Barth, A. J., 2001, ApJ, 556, 75
Nagar, N. M., Falcke, H., Wilson, A. S., & Ulvestad, J. S., 2002, A&A, 392, 53
Nagar, N. M., Wilson, A. S., Falcke, H., Ulvestad, J. S. & Mundell C. G., 2002, in "Issues in Unification of AGN", eds. R. Maiolino, A. Marconi, N. Nagar, ASP Conf. Proc., 258, 171
Nandra, K., George, I. M., Mushotzky, R. F., Turner, T. J., & Yaqoob, T., 1997, ApJ, 477, 602
R. Narayan, 2002, In Proceedings of *Lighthouses of the Universe* eds. M. Gilfanov, R. Sunyaev, E. Churazov, (Springer-Verlag, 2002).
Narayan R., Barrett D., & McClintock J. E., 1997,
Narayan R., Igumenschev I. V., & Abramowicz M. A., 2000, ApJ, 539, 798
Narayan, R., Mahadevan, R., & Quataert, E., 1998b, in *Theory of Black hole accretion disks*, eds. M.A. Abramowicz, G. Bjornsson, and J.E. Pringle. (CUP, 1998)

Narayan R., Quataert, E., Igumenschev I. V., & Abramowicz M. A., 2002, ApJ, 577,295
Narayan, R. & Yi, I., 1994, ApJL, 428, L13
Narayan R. & Yi I., 1995, ApJL, 452, 710
Oshlack A. Y. K. N., Webster R. L., & Whitting M. T., 2002, ApJ, 576, 81
O'Dea C. P., 1998, PASP, 110, 493
Orosz, J. A. & Bailyn, C. D., 1997, ApJ, 477, 876
Pellegrini, S., Venturi, T, Comastri, A., Fabbiano, G., Fiore, F., Vignali, C., Moragnti, R., & Trincheri, G., 2003, ApJ, 585, 677
Polletta, M., Bassani, L., Malaguti, G., Palumbo, G. G. C.& Caroli, E., 1996, ApJS, 106, 399
Pounds, K., Reeves, J., O'Brien, P., Page, K., Turner, M., & Nayakshin, S., 2001, ApJ, 559, 181
Press, W. H., Teukolsky, S. A., Vetterling, W. T., & Flannery, B. P., 1992, *Numerical Recipes* (2nd ed.; Cambridge: CUP)
Quataert E. & Narayan R., 1999, ApJ, 520, 298
Rawlings S. & Saunders R., 1991, Nature, 349, 138
Rees M. J., Phinney E. S., Begelman M. C., & Blandford R. D., 1982, Nature, 295, 17
Rush, B., Malkan, M. A., & Edelson, R. A., 1996, ApJ, 473, 130
Rybicki G. B. & Lightman A. P., 1979, *Radiative processes in astrophysics* (New York: Wiley)
Saglia, et al., 1993, ApJ, 403, 567
Sambruna, R. M., Eracleous, M., & Mushotzky, R. F., 1999, ApJ, 526, 60
Sams B. J., Eckart A., & Sunyaev R., 1996, Nature, 382, 47
Schödel, R. et al, 2002, Nature, 419, 694
Shakura, N. I. & Sunyaev, R. A., 1973, A&A, 24, 337
Shih, D. C., Iwasawa, K., & Fabian, A. C., 2003, MNRAS, 341, 973
Simien, F. & Prugniel, Ph., 2002, A&A, 384, 371, and the HYPERLEDA catalogue: http://www-obs.univ-lyon1.fr/hypercat/
Stirling, A. M., Spencer, R. E., de la Force, C. J., Garrett, M. A., Fender, R. P., &Ogley, R. N., 2001, MNRAS, 327, 1273
Tadhunter, C., Marconi, A., Axon, D., Wills, K., Robinson, T. G., & Jackson, N., 2003, MNRAS, 342, 861
Terashima, Y., Iyomoto, N., Ho, L. C., & Ptak, A. F., 2002, ApJS, 139, 1
Terashima, Y. & Wilson, A. S., 2003, ApJ, 583, 145
Thean, A., Pedlar, A., Kukula, M. J., Baum, S. A., & O'Dea, C. P., 2001, MNRAS, 325, 737
Tremaine, S., et al., 2002, ApJ, 574, 554
Turner, T. J. & Pounds, K. A., 1989, MNRAS, 240, 833
Ulvestad, J. S., Antonucci, R. R., & Goodrich, R. W., 1995, AJ, 109, 81
Ulvestad, J. S. & Wilson, A. S., 1989, ApJ, 343, 659
Verlome, E. K. et al., 2002, MNRAS, 335, 517
Véron-Cetty, M. P. & Véron, P., 2001, A&A, 374, 92
Wagner, R. M., Foltz, C. B., Shahbaz, T., Charles, P. A., Starrfield, S. G., & Hewett, P., 2001, ApJ, 556, 42
Wang, T. & Lu, Y., 2001, A&A, 377, 52
Weaver, K. A., Gelbord, J., & Yaqoob, T., 2001, ApJ, 550, 261
White, N. E., Giommi, P., & Angelini, L., 2000, WGACAT. VizieR On-line Data Catalog: IX/31
Willott C. J., Rawlings S., Blundell K. M. & Lacy M., 1999, MNRAS, 309, 1017
Woo, J. & Urry, C. M., 2002, ApJ, 579, 530
Young, A. J., Wilson, A. C., Arnaud, K. A., Terashima, Y., & Smith, D. A., 2002, ApJ, 564, 176
Zdziarski A. A., Gilfanov M., Lubiński P., & Revnivtsev M., 2003, MNRAS, 342, 355
Zhou, H. & Wang, T., 2002, Chin. J. Astron. Astrophys., 2, 501.

This paper has been typeset from a TEX/ LATEX file prepared by the author.